Fiziksel Buhar Biriktirme ile Grafen Sentezi ve Karakterizasyonu

Uğur Demirkol

YÜKSEK LİSANS TEZİ

Fizik Anabilim Dalı

Haziran 2021

Synthesis and Characterization of Graphene by Physical Vapor Deposition

Uğur Demirkol

MASTER OF SCIENCE THESIS

Department of Physics

June 2021

Synthesis and Characterization of Graphene by Physical Vapor Deposition

A thesis submitted to

Eskişehir Osmangazi University

Graduate School of Natural and Applied Sciences

In partial fulfillment of the requirements for the degree of

Master of Science in

The Discipline of Solid State Physics of

The Department of Physics

By

Uğur Demirkol

Supervisor: Assoc. Prof. Dr. Şadan Korkmaz

June 2021

ETHICAL STATEMENT

I hereby declare that this thesis study titled “Synthesis and Characterization of Graphene by Physical Vapor Deposition” has been prepared in accordance with the thesis writing rules of Eskişehir Osmangazi University Graduate School of Natural and Applied Sciences under the academic consultancy of my supervisor Assoc. Prof. Dr. Şadan Korkmaz. I hereby declare that the work presented in this thesis is original. I also declare that I have respected the scientific ethical principles and the rules in all stages of my thesis study, all information and data presented in this thesis have been obtained within the scope of the scientific and the academic ethical principles and the rules, all materials used in this thesis which are not original to this work have been fully cited and referenced, and all knowledge, documents, and results have been presented in accordance with the scientific ethical principles and the rules. 08/06/2021

Uğur Demirkol

Signature

ÖZET

Grafen, karbon atomlarından oluşan sıradışı bir malzemedir ve ilk sentezlenen iki boyutlu malzemedir. Grafen, etkileyici fiziksel özelliklerine ve büyük ölçekte ucuz bir şekilde üretilebilmesine rağmen, teknolojik cihazlarda kullanımı hala kısıtlıdır. Bu durum grafenin mevcut sentez yöntemlerinin diğer yarı-iletken üretim yöntemleriyle uyumlu olmamasından kaynaklanmaktadır. Diğer işlemlerin gereksinimlerini karşılayacak yeni grafen sentezi yöntemlerinin geliştirilmesi gerekmektedir.

Çalışmamızın amacı, oda sıcaklığına yakın bir sıcaklıkta yeni bir grafen sentez yöntemi geliştirmektir. Çalışmalarımızı gerçekleştirmek için fiziksel buhar biriktirme yöntemlerinden biri olan termiyonik vakum ark tekniği kullanılmıştır. Örnekler üretilip, Raman spektroskopisi ile incelenerek çeşitli yaklaşımlar denenmiştir. Çalışmamız boyunca üretilen örneklerin Raman spektrumlarında termiyonik vakum ark tekniği ile bir geçiş metali tabakası kaplanması sonrasında sp^3 hibritleşmesine sahip karbon bağlarının sp^2 hibritleşmesine sahip karbon bağlarına katalizi gözlenerek ispatlanmıştır. Çalışmanın kapsamındaki son yaklaşımla üretilen örneklerin Raman spektrumları çok katmanlı grafen ile benzer sonuçlar göstermiştir.

Anahtar Kelimeler: Grafen, İki Boyutlu Malzemeler, Fiziksel Buhar Biriktirme, Termiyonik Vakum Ark, Raman spektroskopisi

SUMMARY

Graphene is an extraordinary material made of carbon atoms and the first synthesized two-dimensional material. Although graphene has impressive physical properties and can be produced on a large scale at a low cost, the use of graphene in technological devices is still limited due to the incompatibility of current synthesis methods with other manufacturing processes of semiconductor devices. New graphene synthesis methods must be developed with respect to the needs of other processes.

The aim of this study was to create a new method of synthesizing graphene at near room temperature. In order to achieve that thermionic vacuum arc technique, which is a physical vapor deposition method with huge advantages, was utilized to conduct our studies. Various deposition approaches have been tested by producing samples and investigating with Raman spectroscopy. It is proven that throughout the study, the Raman spectra of the samples produced showed the catalysis of carbon bonds with sp^3 hybridization into carbon bonds with sp^2 hybridization after deposition of a transition metal layer with thermionic vacuum arc technique. The Raman spectra of the samples produced with the final approach tested in the scope of this study showed similar results as multi-layer graphene.

Keywords: Graphene, Two-Dimensional Materials, Physical Vapor Deposition, Thermionic Vacuum Arc, Raman Spectroscopy

LIST OF CONTENTS

Page

LIST OF CONTENTS (Continued)

Page

LIST OF FIGURES

Figure **Page**

LIST OF ABBREVIATONS AND SYMBOLS

Symbols	Descriptions
A	Ampere
Å	Angstrom
a_1, a_2	Lattice Unit Vectors
b_1, b_2	Reciprocal Lattice Unit Vectors
C_2H_2	Acetylene
C_2H_4	Ethylene
CH_4	Methane
cm	Centimeter
CO_2	Carbon Dioxide
° C	Celsius
E	Energy
eV	Electron Volt
GPa	Gigapascal
H	Hamiltonian
ħ	Reduced Planck Constant
H.c.	Hamiltonian Constant
H_2	Hydrogen
h-BN	Hexagonal Boron Nitride
I	Intensity
k	Wave Vector
K	Kelvin
m	Meter
µm	Micrometer
N	Number of Atoms per Unit Cell
N_2	Nitrogen
$NaBH_4$	Sodium Borohydride
nm	Nanometer

LIST OF ABBREVIATIONS AND SYMBOLS (Continued)

Symbols	**Descriptions**
Pa	Pascal
s	Second
SiC	Silicon Carbide
SiO_2	Silicon Dioxide
TPa	Terapascal
V	Volt
v_F	Fermi Velocity
W	Watts
$\Delta\tilde{\nu}$	Raman Shift
λ	Wavelength
π	Pi
σ	Sigma, Pauli Spin Matrix
Ω	Ohm

Abbreviations	**Descriptions**
0D	Zero-Dimensional
1D	One-Dimensional
2D	Two-Dimensional
3D	Three-Dimensional
CCD	Charge-Coupled Device
CMOS	Complementary Metal-Oxide-Semiconductor
CNT	Carbon Nanotube
CVD	Chemical Vapor Deposition
DI	Deionized
DLC	Diamond-Like Carbon
FTIR	Fourier-Transform Infrared Spectroscopy
GIC	Graphene Intercalated Compound

LIST OF ABBREVIATONS AND SYMBOLS (Continued)

Abbreviations	Descriptions
GO	Graphite Oxide
HOPG	Highly Oriented Pyrolytic Graphite
IR	Infrared
iTA	In-Plane Transverse Acoustic
iTO	In-Plane Transverse Optical
LO	Longitudinal Optical
MEMS	Microelectromechanical Systems
Nd:YAG	Neodymium Doped -Yttrium Aluminum Garnet
NEMS	Nanoelectromechanical Systems
oTO	Out-Of-Plane Transverse Optical
PE	Polyethylene
PECVD	Plasma Enhanced Chemical Vapor Deposition
PMT	Photomultiplier Tube
PVC	Polyvinyl Chloride
PVD	Physical Vapor Deposition
RF	Radio Frequency
SAXS	Small-Angle X-Ray Scattering
SEM	Scanning Electron Microscopy
SLG	Single-Layer Graphene
TEM	Transmission Electron Microscopy
TMDs	Transition Metal Dichalcogenides
TO	Transverse Optical
TVA	Thermionic Vacuum Arc
WAXS	Wide-Angle X-Ray Scattering
XRD	X-Ray Diffraction

1. INTRODUCTION AND PURPOSE

Graphene is a groundbreaking material consists of carbon atoms in two dimensions. It has only one atom thickness. Graphene has a honeycomb lattice with the parameter of 2.46 Å (Novoselov et al., 2004). Graphene is one of the allotropes of carbon (Hirsh, 2010). Carbon is an element, which allows very complex materials to be formed, thanks to its orbital hybridization and strong molecular bonds. It is relatively a small element, which enables four bonds per atom and makes it the perfect ingredient for complex structures. Due to the extraordinary properties of carbon atoms, it is one of the key elements for the existence of life.

The dimensionally restricted materials can show very different properties from their bulk counterparts. This is due to changes in some important parameters, such as the ratio of surface atoms to total atoms, mean free path of charged particles, dipole moments, spatial symmetries, and so on. This phenomenon has changed the perspective of scientists on the physical properties of materials. Before the discovery of graphene and other dimensionally restricted materials, the magnitude of impact on physical properties of dimensional restraints on materials was not comprehended. The two-dimensional materials were the first dimensionally restricted materials, and graphene was the first two-dimensional material to be discovered. To understand better, graphene and graphite can be compared. Graphite is a material made of carbon atoms arranged in a hexagonal crystal structure. Graphite is the three-dimensional allotrope of graphene. If the atomic layers are separated in graphite, the separated layers are simply graphene layers. Both in graphene and graphite intra-layer carbon-to-carbon bond length is 1.42 Å. The bond length between layers in graphite is 3.35 Å (Delhaes, 2000). The electrical conductivity of graphite at room temperature is anisotropic and the electrical conductivity perpendicular to the hexagonal axis (along the basal plane) is around 10^6 Ω^{-1} m^{-1} and the electrical conductivity parallel to the hexagonal axis is around 100 Ω^{-1} m^{-1} (Dutta, 1953). However, the electrical conductivity of isolated graphene at room temperature is around $10^7 - 10^8$ Ω^{-1} m^{-1}, which is nearly 100 times higher than its three-dimensional counterpart graphite (Marinho et al., 2012). The mechanical strength can be compared as well. The Young's modulus of graphite is around 1 TPa along the basal plane, but perpendicular to the basal plane the Young's modulus is around 30 GPa and the Young

modulus of graphene is around 1 TPa (Chang and Chen, 2015). Since there is not an additional plane for graphene, graphene is a stronger material than graphite. If the thermal conductivities of both materials are investigated, it is clear that graphene has better thermal conductivity than graphite. At room temperature, the thermal conductivity perpendicular to the basal plane of graphite is 2 W m^{-1} K^{-1}, and along the basal plane is 2195 W m^{-1} K^{-1}, and 3541 W m^{-1} K^{-1} for graphene (Alofi and Srivastava, 2013). There are many tremendous aspects discovered of this material, yet there are many aspects that await studying.

These extraordinary properties of two-dimensional materials have the potential for enabling to overcome the problems of traditional devices such as three-dimensional semiconductor-based transistors, sensors, and other technologies limited by the physical restrictions of three-dimensional materials. These problems include slow heat dissipation in devices, physical size limits of the depletion width in p-n junctions of semiconductors, non-tunable band gaps, and many more. With new manufacturing technologies, smarter devices can be produced using two-dimensional materials. In order to pave the way that leads to new technologies, new synthesis methods that are easy, low-cost, and most importantly integrable to other manufacturing processes are needed. This study aims to create an alternative and improved synthesis method of graphene.

In this study, new techniques and approaches have been developed for the synthesis of graphene with a physical vapor deposition method, the thermionic vacuum arc (TVA) technique. All the samples produced in this study were investigated with Raman spectroscopy.

2. LITERATURE REVIEW

2.1. Hybridization of Carbon

Carbon has the atomic number of six, which means it consists of six electrons, six protons, and the number of neutrons between six and eight. Only two electrons can occupy a single energy state, due to Pauli Exclusion Principle (Pauli, 1925). At the ground state, the electrons of a carbon atom can occupy 1s, 2s, and 2p atomic orbitals. 1s and 2s energy states of a single carbon atom at ground state are occupied with 2 electrons each and the remaining 2 electrons occupy 2p energy states. When a carbon atom bonds with other atoms, this electronic structure changes, and 2s energy state begins to merge with 2p energy states. This is called the hybridization of orbitals (Pauling, 1931). This allows carbon atoms to make bonds with different angles thus allowing them to form various crystal lattices. There are 3 different orbital hybridizations that can occur with carbon atoms. If 2s and $2p_x$ energy states form a new hybrid energy state, the bond angle becomes 180°. This hybridization is called "sp hybridization" due to the fact it is consists of a s energy state and a single p energy state and is shown in Figure 2.1(b). This hybridization is seen with carbon dioxide (CO_2), acetylene (C_2H_2), and various molecular bonds. Likewise, when 2s, $2p_{x,}$ and $2p_y$ energy states form a new hybrid state, the bond angle becomes 120°. With the same analogy, this is called "sp^2 hybridization" and is given in Figure 2.1(c). Ethylene (C_2H_4), graphite and importantly graphene molecular bonds can be given examples of sp^2 hybridization. Lastly, when 2s, $2p_x$, $2p_{y,}$ and $2p_z$ energy states form a new hybrid state, the bond angle becomes 109.5°. Also, this is called "sp^3 hybridization" where it is seen in diamond, methane (CH_4), and various molecular bonds and also is illustrated in Figure 2.1(d).

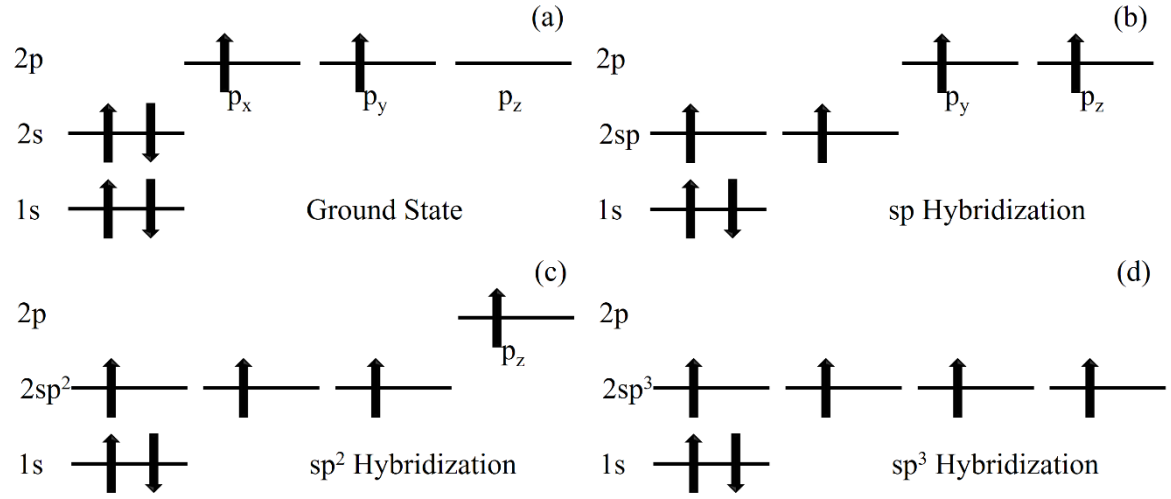

Figure 2.1: Hybridization of carbon atoms, carbon atom orbitals at a) ground state, b) sp hybridization, c) sp^2 hybridization and d) sp^3 hybridization

sp^2 hybridization holds special importance for this research. The molecular bonds, which are derived from sp^2 hybrid orbitals, are strong and chemically stable covalent bonds called sigma (σ) bonds. As mentioned before, these bonds have a 120° angle between them, thus enabling the hexagonal lattice in two dimensions, as well as strong tensile strength and high Young's modulus (Papageorgiou et al., 2017). In addition to these bonds, there is another covalent bond, which originates from the p_z orbital, which is called the pi (π) bond. These bonds are relatively weaker than σ bonds. Four sigma bonds appear when a carbon atom is in sp^3 hybridization state and forms a compound such as methane and diamond; three sigma and one pi bonds appear when a carbon atom is in sp^2 hybridization state and forms a compound such as graphite and benzene, and finally, two sigma and two pi bonds appear when a carbon atom is in sp hybridization state and forms a compound such as acetylene. In graphite, these π bonds are essential to keep hexagonal graphene layers on top of each other; but if you separate the layers of graphite, p_z orbitals will form double bonds with nearest carbon atoms. These π bonds can easily orient themselves within crystal structure by changing the electronic configuration. This results in magnificent electrical and thermal conductivity and charge carriers to become "massless Dirac fermions" which is explained later (Novoselov et al., 2005).

2.2. Carbon Allotropes and Crystal Structure of Graphene

An allotrope defines one of the materials, which possess the same element but different crystal structures with different physical properties. Carbon is an element, which can form the most complex molecular structures in the universe and has the most number of allotropes. Diamond, graphite, lonsdaleite, fullerene, carbon nanotubes, carbyne, and graphene are the most noticeable allotropes of carbon atoms (Dinadayalane and Lesczyski, 2010). Due to various hybridization of carbon atomic orbitals, carbon can bond with neighboring carbon atoms at different angles. The molecular bond degree of 120° angle in sp^2 hybridization can make the carbon atom form hexagonal structures such as graphite, graphene, carbon nanotubes, and fullerene. The different allotropes of hexagonal carbon are shown in Figure 2.2 where zero-dimensional (0D) form Buckminsterfullerene can be seen in Figure 2.2(a), one-dimensional (1D) form carbon nanotube (CNT) is illustrated in Figure 2.2(b), two-dimensional form graphene is shown in Figure 2.2(c) and lastly three-dimensional (3D) form graphite can be seen in Figure 2.2(d).

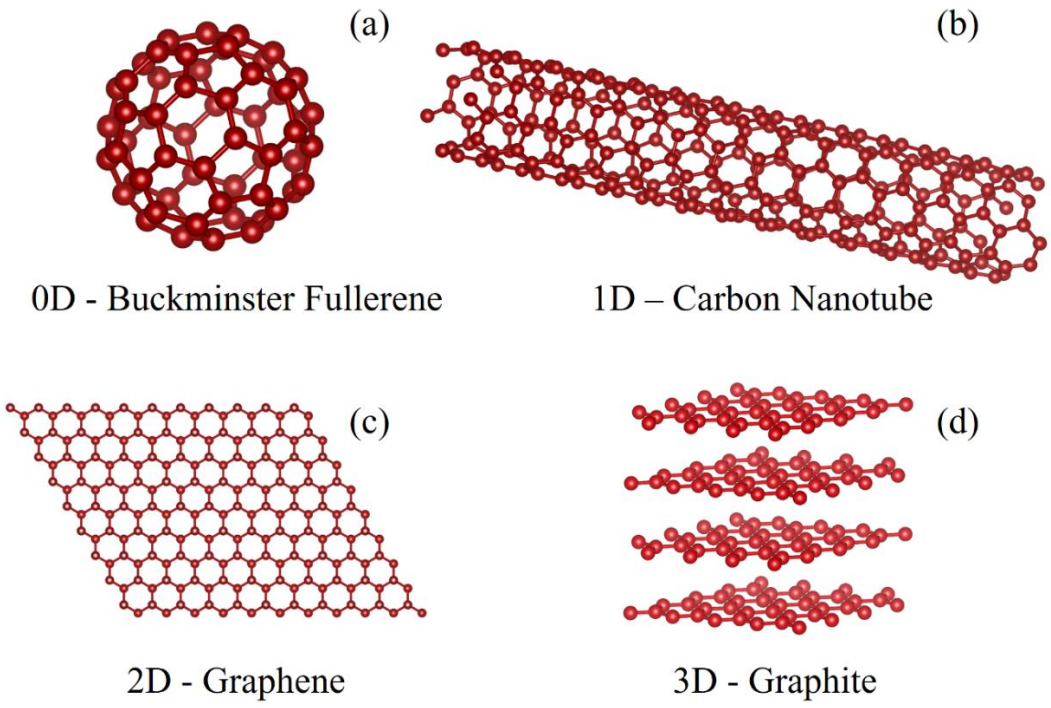

Figure 2.2: Allotropes of hexagonal carbon atoms: a) Buckminsterfullerene, b) Carbon nanotube, c) Graphene and d) Graphite

2.3. Two – Dimensional Materials

All materials are lying within three dimensions but at the nanoscale, they might have some restricted degree of freedom for some specific dimensions. For instance, if one thinks of an electron passing through a metal wire, it can move freely along the length of the wire; but its movement is restricted along the width of the wire where the movement is only limited within the diameter of the wire. At the metric scale, it can be thought as the wire has only one dimension, whereas a sheet of metal has two dimensions and a metal bar has three dimensions. At the nanoscale, only a dozen of atoms are enough to remove dimensional restrictions. In retrospect, it means the restricted dimension can only be thick as few atoms at the nanoscale. In Figure 2.2 where the carbon allotropes are shown, it is also shown how different structures are restricted dimension-wise. A material that is restricted in only one dimension is called “Two – Dimensional Material”, often abbreviated as “2D material”.

There are various 2D materials, which can be grouped as Xenes, Transition Metal Dichalcogenides (TMDs), MXenes, and MAXenes; along with some other materials like hexagonal boron nitride (h-BN). The suffix “-ene” is derived from graphene, where its bulk form is graphite, to create a vocal similarity to describe a 2D material (Xu et al., 2013).

The word “Xene” is used to describe a monoelemental material that forms a 2D structure. Beyond graphene; IV-A, V-A, and some of III-A group elements can form two-dimensional monoelemental structures, such as silicone (silicon), germanene (germanium), stannene (tin), plumbene (lead), phosphorene (phosphorus), arsenene (arsenic), antimonene (antimony), bismuthene (bismuth), borophene (boron) and gallenene (gallium) (Miró et al., 2014).

Transition Metal Dichalcogenides refer to materials, which consist of one transition metal atom such as tungsten, molybdenum, titanium, which have partially filled d sub-shell, and two chalcogenide atoms such as sulfur, selenium, tellurium, and polonium. TMDs have gained lots of attention due to their properties, which are available in 2D such as direct band

gap of some TMDs, spin-orbit coupling, and allowing new technologies as valleytronics (Wang et al., 2012).

MXene and MAXene also refer to materials, which have transition metal atoms in their structure. Abbreviations in 2D materials are generally derived from certain elemental groups in the periodic table and MAXene and MXene are not different from this perspective. “M” letter is attributed to early transition metals such as titanium, vanadium, and chrome; “A” letter is attributed to A-group elements, mostly from III-A and IV-A groups, such as aluminum, gallium, silicon, and indium. “X” letter refers to carbon and nitrogen atoms separately or as mixed. These structures also can be terminated with functional groups such as oxygen, fluorine, hydroxide, and chlorine. MXene and MAXene are generally metallic and show good physical properties, which makes them suitable for battery and filtration technologies (Khazaei et al., 2013).

2.4. Electronic Properties of Graphene

Electronic properties of single-layer graphene can be derived from the tight-binding approach. The tight-binding approach can be described as a semi-empirical method to calculate the electronic structure of solid-state materials by defining wave functions and their superpositions and calculating single-particle Bloch states of a material. In simpler words, instead of calculating the electronic structure of the whole material, calculating the electronic structure of a single atom and its nearest neighbors (Wallace, 1947). The honeycomb structure of graphene and its Brillouin zone is shown in Figure 2.3 where on the left side honeycomb lattice is shown. Every edge of hexagon represents a carbon atom and a_1 and a_2 vectors are lattice unit vectors. On the right side of Figure 2.3, the Brillouin zone of graphene and its reciprocal-lattice vectors in momentum space is illustrated. K, M, and Γ points represent the middle of an edge joining two hexagonal faces, the center of a hexagonal face and the center of the Brillouin zone, respectively.

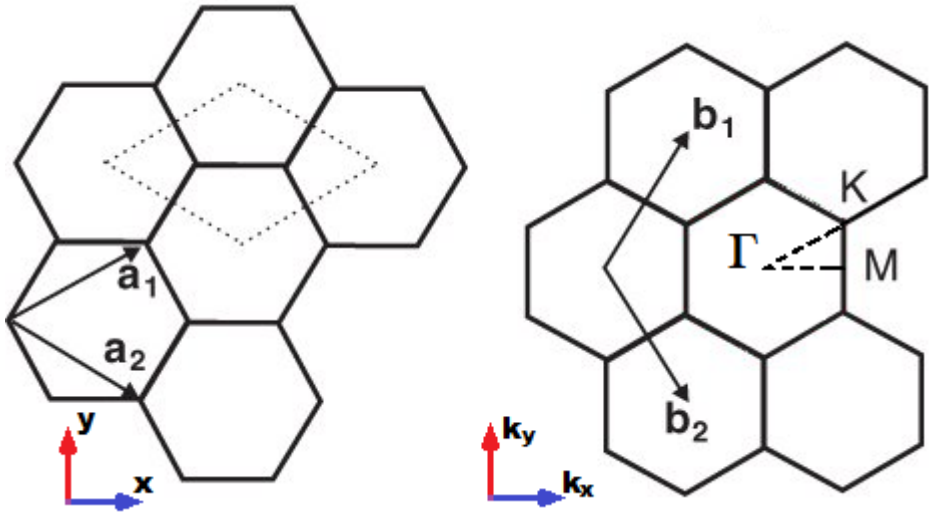

Figure 2.3: Honeycomb lattice of graphene and its Brillouin zone.

The honeycomb lattice of graphene can be seen as a triangular lattice with two carbon atoms per unit cell. The carbon to carbon distance of this lattice is near 1.42 Å. Lattice vectors of graphene are shown below along with its reciprocal-lattice vectors.

$$\boldsymbol{a}_1 = \frac{a}{2}(3,\sqrt{3})\,, \qquad \boldsymbol{a}_2 = \frac{a}{2}\,(3,-\sqrt{3}) \tag{2.1}$$

$$\boldsymbol{b}_1 = \frac{2\pi}{3a}(1,\sqrt{3})\,, \qquad \boldsymbol{b}_2 = \frac{2\pi}{3a}(1,-\sqrt{3}) \tag{2.2}$$

Corners of Brillouin zone of graphene, K and K', hold special importance, which will be discussed later. Their positions in momentum space are given below.

$$\boldsymbol{K} = \left(\frac{2\pi}{3a},\frac{2\pi}{3\sqrt{3}a}\right)\,, \qquad \boldsymbol{K'} = \left(\frac{2\pi}{3a},-\frac{2\pi}{3\sqrt{3}a}\right) \tag{2.3}$$

For tight-binding model calculations, one also should consider neighbor vectors into account. Three nearest neighbor vectors in real space are:

$$\boldsymbol{\delta}_1 = \frac{a}{2}(1,\sqrt{3}) \qquad \boldsymbol{\delta}_2 = \frac{a}{2}(1,-\sqrt{3}) \qquad \boldsymbol{\delta_3} = -a(1,0) \tag{2.4}$$

The next-nearest neighbor vectors, which are also useful in our calculations, are given below.

$$\boldsymbol{\delta}_1' = \pm\boldsymbol{a}_1 \qquad \boldsymbol{\delta}_2' = \pm\boldsymbol{a}_2 \qquad \boldsymbol{\delta}_3' = \pm(\boldsymbol{a}_2 - \boldsymbol{a}_1) \tag{2.5}$$

In the tight-binding model, it is assumed that electrons can jump between nearest and next-nearest atoms with a specific hopping energy. If one writes the tight-binding Hamiltonian for electrons in graphene and uses units such as $\hbar = 1$, the Hamiltonian would be similar to the one below (Neto et al., 2009).

$$H = -t\sum_{\langle i,j\rangle,\sigma}\left(a_{\sigma,i}^{\dagger}b_{\sigma,j} + \text{H.c.}\right) - t'\sum_{\langle\langle i,j\rangle\rangle,\sigma}\left(a_{\sigma,i}^{\dagger}a_{\sigma,j} + b_{\sigma,i}^{\dagger}b_{\sigma,j} + \text{H.c.}\right) \tag{2.6}$$

In the equation 2.6, $a_{i,\sigma}(a_{i,\sigma}^{\dagger})$ creates or annihilates an electron with spin σ ($\sigma = \uparrow, \downarrow$) on a sublattice, t is the nearest neighbor hopping energy between different sublattices which is around 2.8 eV, t' is the next-nearest neighbor hopping energy in the same sublattice which is between $0.02t$ and $0.2t$ (Reich et al., 2002) but from ab-initio calculations, it is estimated around 0.1 eV (Deacon et al., 2017) and H.c. is Hamiltonian constant. If this tight-binding Hamiltonian is solved and energy bands derived, the energy equation would become the one below.

$$E_{\pm}(\mathbf{k}) = \pm t\sqrt{3 + f(\mathbf{k})} - t'f(\mathbf{k}) \tag{2.7}$$

$$f(\mathbf{k}) = 2\cos\left(\sqrt{3}k_y a\right) + 4\cos\left(\frac{\sqrt{3}}{2}k_y a\right)\cos\left(\frac{3}{2}k_x a\right) \tag{2.8}$$

The plus sign in the energy equation represents the upper π^* band and the negative sign represents the lower π band. If the next-nearest hopping energy t' is zero, the energy band becomes symmetrical around zero energy. For values of t' other than zero, the electron-hole symmetry is interrupted and π and π^* bands become asymmetric. If the energy equation is calculated, while t and $t'$are finite numbers ($t = 2.7$ eV and $t' = -0.2t$), Energy spectrum across k_y and k_x would be plotted as in Figure 2.4.

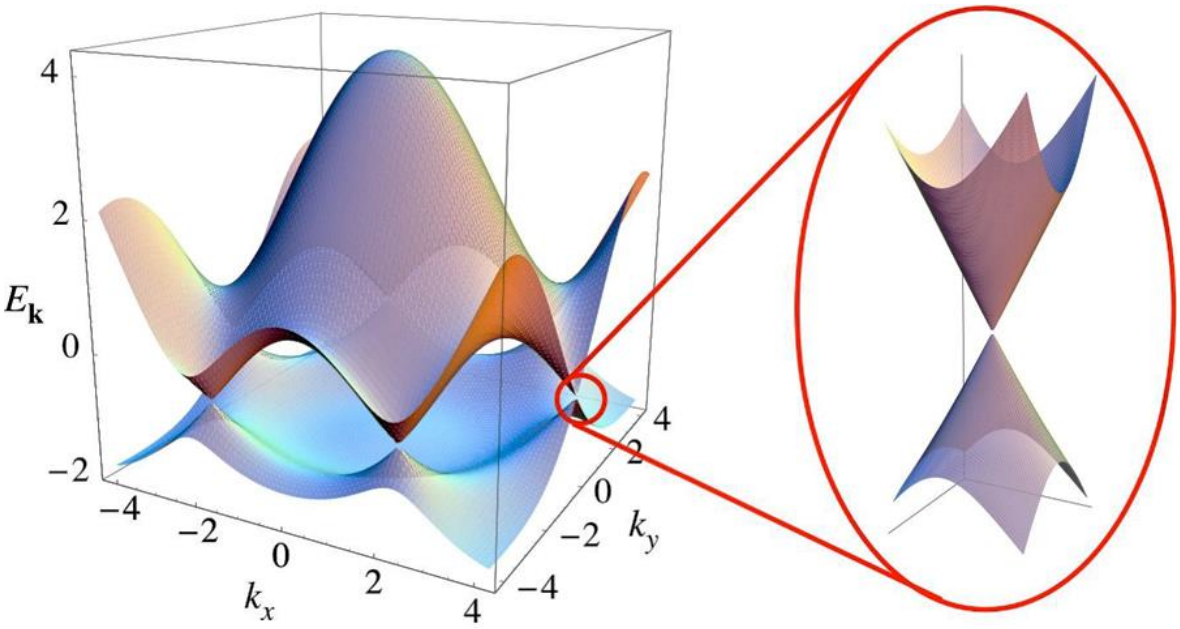

Figure 2.4: Electronic dispersion of honeycomb lattice of graphene. Right: Zoomed energy spectrum at K point, showing Dirac point (Neto et al., 2009).

As can be seen in Figure 2.4, K and K' points hold special importance. Band structure at these points is symmetrical and valence and conduction bands are connected at zero energy. These points are called Dirac points and the band structure around Dirac point is called Dirac cone. Fermi velocity (v_F) is estimated around $1 \times 10^6 \mathrm{m/s}$ (Wallace, 1947).

Dirac cones occur when valence and conduction bands are shaped like two halves of a conical surface and meets at Dirac point at Fermi energy (Geim and Novoselov, 2010). This band structure is present at the band structure of topological insulators, which are materials that behave as insulators inside but on the surface they have conducting states that make them conduct electrons. Graphene is also a topological insulator, due to its two-dimensional nature, charge transport only occurs on its surface (Hasan and Kane, 2010). Due to Dirac cones, electrical conduction is carried by massless Dirac fermions, which is explained by solving the relativistic Dirac equation (Fujita et al., 1996). The term "massless" is derived from the fact that cyclotron mass in graphene, varies with Fermi velocity and electronic density, hence being independent of the mass of the charge carriers (Neto et al., 2009).

Pristine graphene is a very good electrical conductor, since its valence and conduction bands meet at Fermi energy at K and K' points, as shown in Figure 2.5(a). Doping or stacking layers can easily manipulate this electronic configuration of graphene. n-type doping of graphene, where electron-hole balance is disturbed with excess electrons coming from electron donor dopant atoms, hence creating electron dominant charge configuration; causes Fermi energy level to shift into the conduction band, which is illustrated in Figure 2.5(b). Similarly, p-type doping of graphene, where electron-hole balance is disturbed with the extraction of electrons by electron acceptor dopant atoms, hence creating hole dominant charge configuration; causes Fermi energy level to shift into valence band, which is shown in Figure 2.5(c) (Liu et al., 2011).

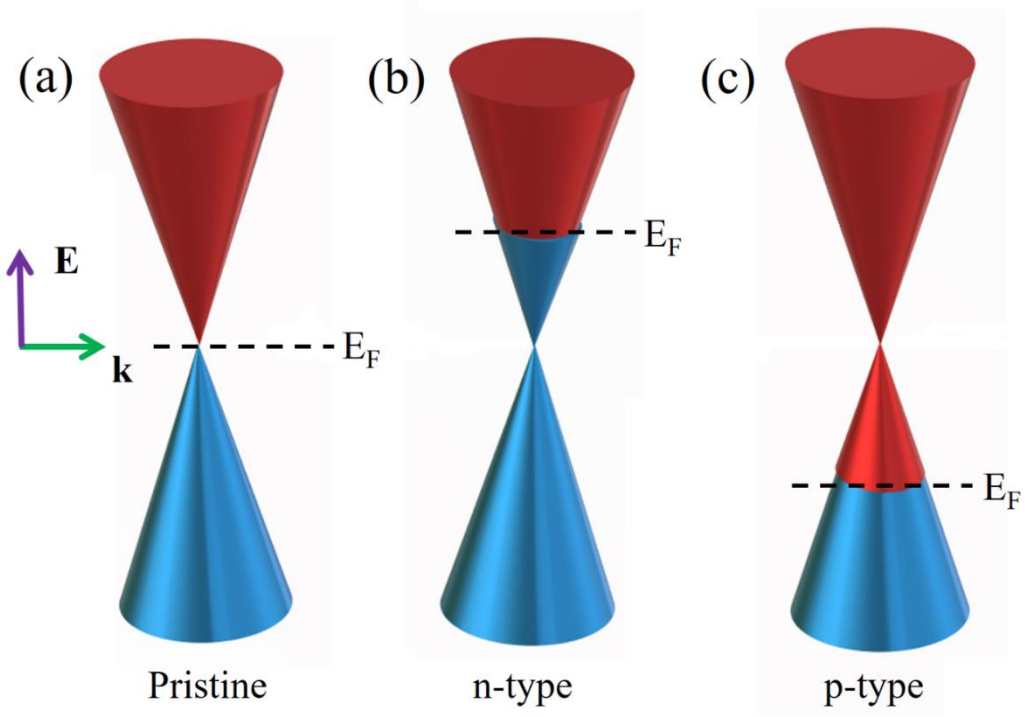

Figure 2.5: Schematic electronic band structure of graphene at K and K' points for a) pristine graphene, b) n-type doped graphene and c) p-type doped graphene.

In addition to the interesting electronic properties of graphene, superconductivity was achieved by stacking graphene layers with a special twist angle at 1.7 K temperature (Cao et al., 2018).

2.5. Synthesis Methods of Graphene

Synthesis of graphene was started as deposition of few layers of graphite onto transition metals in the 1970s (Eizenberg and Blakely, 1979 a; Eizenberg and Blakely, 1979 b). In 1975, few layers of graphite were synthesized in single-crystal form onto platinum by using chemical decomposition methods; but it was not named as graphene (Lang, 1975). This was due to the fact; there was a lack of characterization techniques and a lack of field of applications. Besides, in those years, due to the difficulty of transferring and abstracting such materials on insulating substrates, their electronic properties could not be adequately studied.

In the late 1990s, Ruoff and his team have tried to extract and insulate graphite layers by mechanically scraping Highly Oriented Pyrolytic Graphite (HOPG) onto silicon dioxide (SiO_2) substrates; but they did not investigate its electrical properties (Lu et al., 1999). By using a similar method Kim and his team investigated electronic properties (Zhang et al., 2005). In 2004, Geim and his co-workers were able to successfully abstract graphene and insulate on SiO_2 substrate. With this research, they investigated the electronic properties of graphene and attracted many scientists in this field of research, and gained huge momentum (Novoselov et al., 2004). In 2004 and 2005; graphene, molybdenum disulfide, niobium diselenide, and hexagonal boron nitride two-dimensional layers were able to be separated from their bulk counterparts (Novoselov et al., 2005). First produced graphene was synthesized by mechanical exfoliation method, using adhesive tape. While the method was cheap, easy, and produces good quality graphene flakes, new methods were required due to small micron-sized flakes (Bhuyan et al., 2016).

There are many synthesis methods of graphene. The methods are grouped in two sections as “top-down” and “bottom-up” methods due to their production approach. In the “top-down” method, graphene flakes are separated from bulk graphite and graphite variants such as graphite oxide and graphite fluoride; whereas in “bottom-up” methods, carbon atoms are arranged so that it creates graphene layers.

2.5.1. Mechanical exfoliation

It is possible to create single-layer graphene flakes with the mechanical exfoliation method. While this method is rarely used, graphene flakes with high quality can be produced. Highly oriented pyrolytic graphite, single-crystal graphite, or natural graphite has weak interlayer van der Waals bonds. These bonds can be broken mechanically, thus leading to create single-layer graphene flakes. Mechanical exfoliation method can be used by separating graphene layers with adhesive tape (Novoselov et al., 2004), ultrasonication (Xia et al., 2013), electrical field (Liang et al., 2009), or transfer printing technique (Liang and Chou, 2007). Graphene produced by using patterned gold thin films and HOPG is both a cheap and high-quality product but is hard to obtain and its applications are limited.

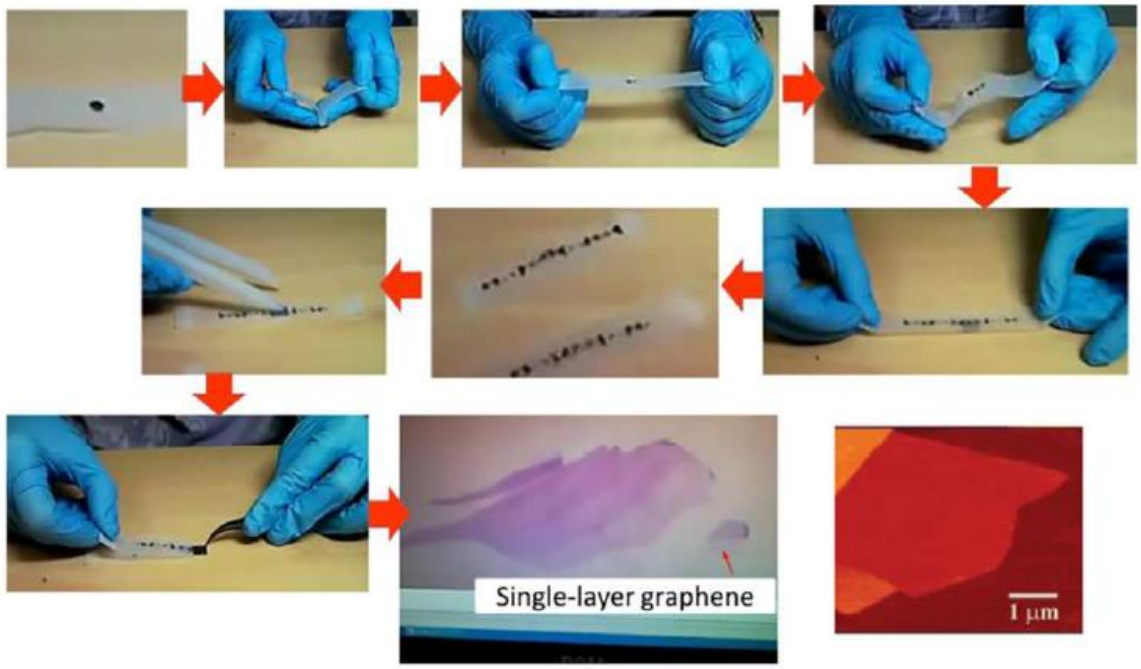

Figure 2.6: Graphene sample produced by placing graphite on adhesive tape and separating layers step by step (Yi and Shen, 2015).

2.5.2. Chemical exfoliation

The chemical exfoliation method is based on preparing colloidal solution from graphite and graphitic compounds. This method is conducted within two stages. Firstly,

weak van der Waals bonds are weakened even further, so the distance between layers is increased. This is a necessary step to allow various radicals to enter between layers. Later on, graphene intercalated compounds (GICs) are produced by different chemical reactions. Finally, these GICs are heated rapidly or separated by ultrasonication to produce graphene flakes (Wu et al., 2010).

2.5.3. Reduced graphene oxide

Producing large quantities of graphene is no small task, but helpfully chemically reducing graphene oxide to produce graphene flakes makes the task easier. Graphite oxide (GO) is usually produced by oxidizing graphite with concentrated sulphuric acid, nitric acid, potassium permanganate as similar to Brodie's method (Brodie, 1859), Hummers' method (Hummers and Offeman, 1958), Staudenmaier's method (Staudenmaier, 1898) and similar oxidizing agents and techniques. Later on, produced GO is reduced chemically. In a system with large amounts of reducing agents such as sodium borohydride ($NaBH_4$) (Shin et al., 2009), hydrogen (H_2) gas is presented to the system, coupled with extrusion of nitrogen (N_2) gas, to reduce GO. Instead of sodium borohydride ($NaBH_4$), other reducing agents such as phenylhydrazine (Pham et al., 2010), hydroxylamine (Zhou et al., 2011), glucose (Zhu et al., 2010), ascorbic acid (Zhang et al., 2010), hydroquinone (Wang et al., 2008), alkaline solutions (Fan et al., 2008) and pyrrole (Amarnath et al., 2011) can be used.

2.5.4. Pyrolysis of graphene

Pyrolysis of graphene is a solvothermal method, which produces graphene by chemical synthesis. Sodium and ethanol are added to a system at a molar ratio of 1:1 in a closed container and the system is heated to the level where thermal reaction can occur. This method is one of the "bottom-up" methods. Graphene layers are then extracted from the pyrolization product, sodium ethoxide by sonication process. Graphene flakes produced by this method show Raman results as similar to defective graphene (Choucair et al., 2009). While this method produces small flakes with dimensions up to 10 μm with lots of defects,

it is desirable since it is cost-friendly and can be conducted at relatively low temperatures (Speyer et al., 2018).

2.5.5. Chemical vapor deposition

Chemical vapor deposition (CVD) is a "bottom-up" chemical process, where precursor molecules are heated and transformed into a gaseous state, which can form desired product by various chemical reactions. For graphene synthesis, the CVD process includes transition metal substrates where it acts as a catalyst to disintegrate and dissolve heated precursors at a high temperature. Precursors, which contain carbon atoms such as methane, ethanol, and other forms of hydrocarbon compounds, react with annealed transition metals at sintering temperatures and disintegrate into carbon atoms. These carbon atoms dissolve either inside the transition metal substrate as nickel substrate or on the surface of the transition metal substrate as copper substrate. After introducing carbon precursor to the system and the cooling process begins, carbon atoms form graphene flakes on the surface of the substrates. All this process is generally accompanied by other inert gases such as argon for flushing oxygen from the system to prevent oxidation; and hydrogen gas for terminating the edges of graphene flakes to reduce interaction with the substrate after forming (Zhang et al., 2014). Transition metal substrates generally define layer number and characteristic properties of graphene flakes. This is mainly due to the different catalysis processes of different transition metals. While nickel (Kim et al., 2009) and copper (Reina et al., 2009) are generally used as substrates, other transition metals such as palladium (Choucair et al., 2009), ruthenium (Sutter et al., 2008), and iridium (Coraux et al., 2008) can also be used. The studies of graphene synthesis on a large area with the CVD method began around 2008, using nickel as substrate (129). Prior to these studies, in 1966, methane was introduced to nickel substrate at $T = 900\,^{\circ}C$ to obtain a thin graphite bed to support samples in electron microscopy (Karu and Beer, 1966). In 1971, few-layer graphene was obtained by evaporating a graphite rod on copper surfaces (Perdereau and Rhead, 1971). In 1975, monolayer graphitic material was obtained by the thermal CVD method on a platinum surface (Lang, 1975). Four years later, Blakely and Eizenberg successfully acquired graphite layers on nickel (111) substrates (Eizenberg and Blakely, 1979). In 1984, the first application, which may be considered as CVD of graphene was achieved onto iridium

substrate, for studying catalytic and thermionic properties of iridium in presence of carbon (Gall et al., 2000). In 2006, graphene synthesis on nickel foil was attempted with the CVD method by using camphor as a precursor compound (Somani et al., 2006). After this study, the CVD method was used for graphene synthesis with various hydrocarbons such as benzene, acetylene, methane, and ethylene as carbon source and different transition metals such as nickel, copper, cobalt, gold, and ruthenium as substrate (Reina et al., 2009).

2.5.6. Chemical vapor deposition on copper and nickel foil

Nickel and copper substrates are the most used substrates for graphene synthesis with the CVD method. Nickel absorbs carbon atoms and while cooling down, these carbon atoms are ejected onto the surface of nickel and form graphene flakes (Chae et al., 2009). Since how many carbon atoms dissolving into nickel is unforeseeable, even with the thickness of nickel substrate and precursor flow are controlled, multilayer graphene (a thin film of graphite) is generally obtained by the CVD method using Ni substrate. For some applications, few-layer graphene is desirable and this method is the most used technique. This process is done at 800 – 1000 °C temperature, using H_2, argon, and carbon precursor gases.

The growth mechanism of graphene is different when using a copper substrate. Copper catalyzes carbon precursors and separates carbon atoms. These carbon atoms can be attached to impurities on the surface of a copper substrate, which act as nucleation points for graphene growth (Mattevi et al., 2011). Since graphene growth begins from nucleation points on a copper substrate surface, graphene obtained by the CVD method on a copper substrate generally consists of monolayer graphene flakes with few multilayer graphene zones. This process is conducted at 1035 – 1050 °C temperature, using H_2 gas along with carbon precursor.

Figure 2.7: Chemical vapor deposition furnace for graphene synthesis (MTI Corporation, 2021)

Graphene produced by the CVD method onto transition metal substrates can be transferred to polyethylene (PE) and polyvinyl chloride (PVC) substrates with a lamination machine or any desired surface by coating with photoresists then etching the metal substrate with an acidic solution such as ferric chloride.

2.5.7. Plasma enhanced chemical vapor deposition

The plasma enhanced chemical vapor deposition (PECVD) method is a “bottom-up” process, uses chemical reactions to create desired thin film product. This method is similar to chemical vapor deposition, but instead of heating the chamber externally along with substrates, PECVD uses radio frequency (RF), microwave, and inductive coupling as an energy resource to create energetic plasma from precursor reactive gases to achieve the energy required for the chemical process to start. PECVD method requires less chamber temperature, so it is slightly more suitable for semiconductor devices. Also, this process can be done without using catalyst materials for producing graphene (Shang et al., 2008). The

downside of this method, compared to the CVD method, is the high cost and allows only to use gaseous precursor materials. The first study was completed in 2003, using the PECVD method (Obraztsov et al., 2003). The synthesis of graphene with the PECVD method was achieved on various substrates such as silicon dioxide, silicon, sapphire, molybdenum, zircon, titanium, hafnium, niobium, tungsten, tantalum, copper, and 304 stainless steel. The process generally requires 600 – 900 °C substrate temperature, which is less than the thermal CVD process (Wang et al., 2004).

2.5.8. Epitaxial growth

Epitaxial growth methods use fine delivery of atoms of a crystal structure onto crystallization points such as certain structures or crystal itself, which act as nucleation points, thus regulating the crystal formation process. This method is somewhat similar to the formation of icicles. If water flow is low and the weather is cold enough, liquid water crystallizes into ice from a point and forms an icicle. If water flow is high, there would not be enough time for water molecules to crystalize. Similarly, epitaxial growth methods have relatively slow deposition rates. Epitaxial growth methods are generally separated by their substrate. When the substrate and desired film is of the same material, the process is called “homo-epitaxial growth”; and when the substrate and desired film are different, it is called “hetero-epitaxial growth”. Epitaxial growth of graphene is a hetero-epitaxial growth method since the substrates used are commonly made of silicon carbide (SiC) and rarely made of ruthenium (Sutter et al., 2008). SiC substrates are more advantageous, due to being a wide band gap semiconductor (3 eV). The epitaxial growth of graphene onto SiC substrate is generally carried out on silicon or carbon terminated surfaces of SiC, at around 1300 °C temperature and in ultra-high vacuum (De Heer et al., 2007).

2.5.9. Other techniques

There are few other techniques, which are less used. These techniques include unzipping of carbon nanotubes (CNTs) (Chen et al., 2007), electron beam irradiation of nanofibers (Subrahmanyam et al., 2009), hydrogen arc discharge exfoliation (Wu et al.,

2009), projecting arc discharge onto graphite rods (Panchakarla et al., 2010) and conversion of diamond-like carbon (DLC) thin films into graphene (Subrahmanyam et al., 2008).

2.5.10. Physical vapor deposition with annealing at high temperatures

There are few studies, which achieved forming graphene using physical vapor deposition (PVD) methods, combined with annealing at high temperatures (Narula et al., 2017; Pan et al., 2013; Zheng et al., 2010; Orofeo et al., 2011; Garlow et al., 2016). PVD methods, while being more expensive, are integrable into the modern manufacturing process of electronics. While there are some nuances in these studies, they all depend on the same physics as CVD methods. Instead of introducing carbon atoms with precursor gases, a thin film made of carbon atoms is used as a carbon source. A thin film made of carbon is deposited either onto a substrate or onto the transition metal layer, which was previously deposited onto a substrate. Then, the sample is heated until annealing temperatures (800 – 1200 °C), in an oxygen-free environment. Annealing makes the transition metal layer to catalyze carbon thin film into graphene. The main advantage of this method is being able to form a graphene layer onto any substrate without transferring. Secondly, using photolithographic processes, a thin film made of carbon can be shaped for forming patterned graphene layers. Although PVD methods are promising for synthesizing graphene for electronics, the temperature required for the annealing process to complete is still high for being integrated into semiconductor device processes.

2.5.11. What is next?

The methods of producing graphene respond to the needs of many applications. There are numerous ways to synthesize graphene, but every method has its difficulties. The one area, which needs further studies, is the integration of graphene into semiconductor devices. Most of the techniques are not suitable to known processes of building micro/nanoelectromechanical systems (MEMS/NEMS). Most of the processes are compatible with each other. If an acidic solution corrodes a certain material in the process, the solution is simply not compatible. As in this analogy, most of the methods for the

synthesis of graphene are not compatible. CVD and PECVD methods require too much temperature for semiconductors. Additionally, lithographic processes are a combination of “bottom-up” and “top-down” processes. Any extra transition metal layer such as nickel or copper to form graphene might be impossible to get rid of or patterning graphene with physical etching processes would be futile, due to the highly robust nature of graphene flakes. There are numerous transfer methods of graphene onto the desired substrate as well, but mass production of devices, achieved by transfer methods, would require long production times and workforce. Other methods such as reduction of graphene oxide or arc discharge methods are fast methods to create graphene flakes, but the produced graphene is not in thin film form, which is desirable for lithographic processes. A new method for synthesizing graphene is needed for adding graphene in the mass produced devices.

Semiconductor transistor gates need to be above a certain thickness. This requirement comes from two factors. Firstly, dissipation of heat produced in transistors must be quick, and secondly, due to the quantum tunneling effect, the unwanted charge transitions must be avoided (Hecht, 1989; Keyes, 1975; Markov, 2014). Being atomically thick, having tunable band gap properties with direct transitions, and having incredible conductivity and physical properties; graphene can help to overcome many problems that are seen today in contemporary semiconductor devices. 2D materials are promising forerunners for replacing traditional MEMS/NEMS devices in the future and graphene holds a special place amongst them. These materials need further studies and technologies to unlock their full potentials. Traditional semiconductor technology needs alternative technologies to be future-proof. Scientists all around the world must be ahead of the curve and with the extraordinary properties supplied by 2D materials, new opportunities are yet to come.

3. MATERIALS AND METHODS

3.1. Characterization of Graphene

Graphene can be characterized by using various methods and systems. These methods include X-Ray Diffraction (XRD), Fourier-Transform Infrared Spectroscopy (FTIR), Transmission Electron Microscopy (TEM), Scanning Electron Microscopy (SEM), and Raman Spectroscopy (Wang et al., 2008). While TEM and SEM are both imaging techniques; XRD and its derivatives such as Small-Angle X-Ray Scattering (SAXS) and Wide-Angle X-Ray Scattering (WAXS), FTIR, and Raman Spectroscopy give structural information (Abbandanak et al., 2019). Pristine graphene, being atomically thin and only having C – C bonds, cannot properly be detected and distinguished with XRD and FTIR. Nonetheless, these methods have their benefits as well, since graphene compounds such as graphene oxide and terminated graphene compounds are generally characterized with them (Dikin et al., 2007; Song et al., 2014). Only Raman spectroscopy can give dependable results about pristine graphene (Ferrari et al., 2006). Overall, Raman spectroscopy is the main method for characterizing graphene.

3.1.1. Raman spectroscopy

Raman spectroscopy is a non-destructive spectroscopic characterization method for defining molecular bonds, based on Raman scattering (Raman and Krishnan, 1928). For understanding the mechanism for Raman spectroscopy, Raman scattering needs to be comprehended. Light can scatter from surfaces of matter. Raman scattering is a second-order inelastic scattering process, where momentum is not conserved. When light scatters from a surface of a material, most of the scattered light scatter elastically, which is defined as “Rayleigh Scattering”. When elastic scattering occurs, the frequency of scattered light is equal to incident light. The tiniest fraction (~0.0000001% of Rayleigh scattering) of the scattering process can occur by interacting with other vibrations such as phonons. If Raman scattering occurs with light in the visible spectrum, incident light scatters after interacting at molecular level motions. These motions are consist of translational, rotational, and

vibrational motions. Incident light can lose some of its energy or gain energy by interacting with these molecular motions while scattering (Keresztury et al., 2002). This phenomenon can be thought of as absorption and emission of light between virtual energy levels, which is illustrated in Figure 3.1. When incident light causes molecular motion, it loses a bit of energy and scatters with less energy. This phenomenon is called “Stokes Scattering”. When energy is transferred to the scattering process from molecular motion, scattering light is more energetic than incident light. This phenomenon is called “Anti-Stokes Scattering”. Both Stokes and anti-Stokes Scattering are forms of Raman Scattering. When there is no interaction with molecular motion during scattering, incident and scattering light will have the same energy, which corresponds to “Rayleigh Scattering”.

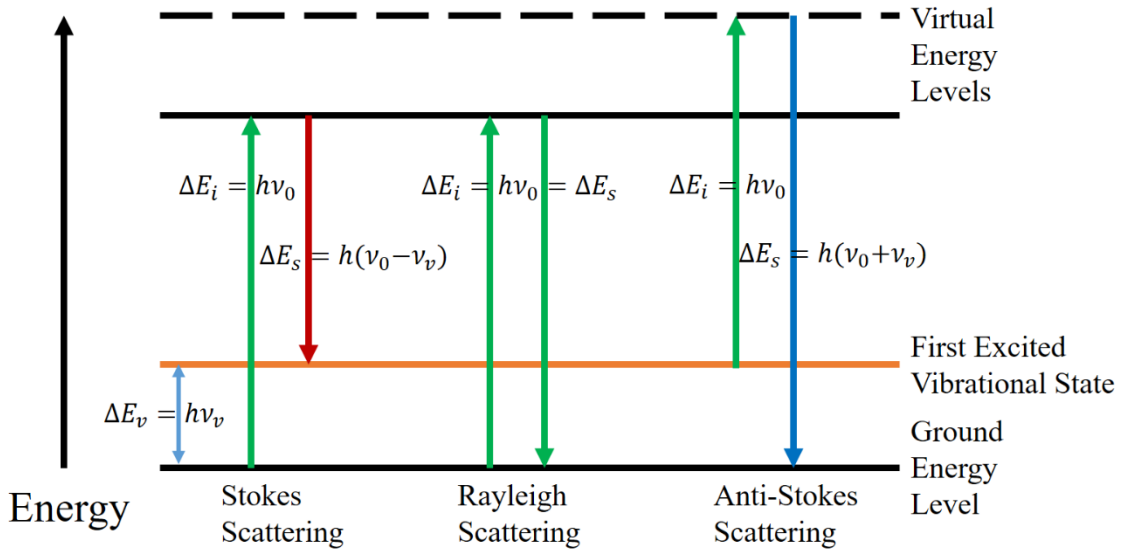

Figure 3.1: Virtual energy diagram along with different scattering processes

Although Raman scattering occurs from all kinds of molecular motion, only centrosymmetric characteristic motions can be detected with Raman spectroscopy. Firstly, the motion must be symmetrical, since non-symmetrical motions would create Raman scattering at random energies without giving characteristic signals. Secondly, the motion must have a center of symmetry, since molecular motions with a center of symmetry cause change in polarizability rather than the dipole moment, so that Raman scattering could occur (Bernath, 2020).

Raman spectroscopy is complementary to Infrared (IR) spectroscopy. Even, there is a rule proposed named “Rule of Mutual Exclusion” between IR spectroscopy and Raman spectroscopy (Venkatarayudu, 1954). This rule states that no normal modes of molecular motion can be visible/active in both Raman and IR spectroscopies. It distinguishes molecular motions as Raman active or IR active. This is due to changes in polarizability, or the dipole moment, caused by molecular motion. If the molecular motion has a center of symmetry, change in polarizability would be dominant and motion would be Raman active. Similarly, if the molecular motion has not a center of symmetry, hence being polar; the change in the dipole moment would be dominant and motion would be IR active. Although, there are molecular motions that are “silent” or “inactive” in both spectroscopies (Keiter, 1983). There are few main differences between Raman spectroscopy and IR spectroscopy. IR spectroscopy relies on absorption of light, instead of scattering. While Raman spectroscopy can use a wide range of the electromagnetic spectrum (from X-rays to near-infrared region), IR spectroscopy can only use infrared spectrum.

Raman spectroscopy is carried out by Raman microscopes, which are devices that consist of a monochromatic light source, optical elements such as lenses, mirrors, and filters for focusing and directing the light, monochromator, and photodetector. Lasers are generally used in Raman microscopes as monochromatic light sources. Diode lasers and Neodymium doped -Yttrium Aluminum Garnet (Nd:YAG) lasers are generally preferred used in Raman microscopes. The type of laser is important since Raman spectroscopy can give different results using different source light. It is wise to use certain source lights that are used frequently in the literature. Most manufacturers of Raman microscopes, knowing this, build in the same types of laser in their products. Monochromatic light sources are required since Stokes and anti-Stokes scattering can only be observed relative to the frequency of incident light. If the incident light is not monochromatic, it would be impossible to separate Raman scattering from Rayleigh scattering caused by a chromatic source. Monochromators also hold importance. A monochromator is a device, which separates the light with a certain wavelength selectively from a chromatic light beam. It is essential for a Raman microscope to detect weak signals coming from Raman scattering. The resolving power of the monochromator used must be high for Raman spectroscopy. The price of Raman microscopes directly correlates with the quality of the monochromator used. Lastly, photodetectors such as charge-coupled devices (CCDs), complementary metal-oxide-

semiconductor (CMOS), and photomultiplier tubes (PMTs); are used to capture the signal coming from Raman scattering. Ideal photodetector for Raman spectroscopy must be highly sensitive, noiseless, and responsive. The main components of a Raman microscope are shown in Figure 3.2.

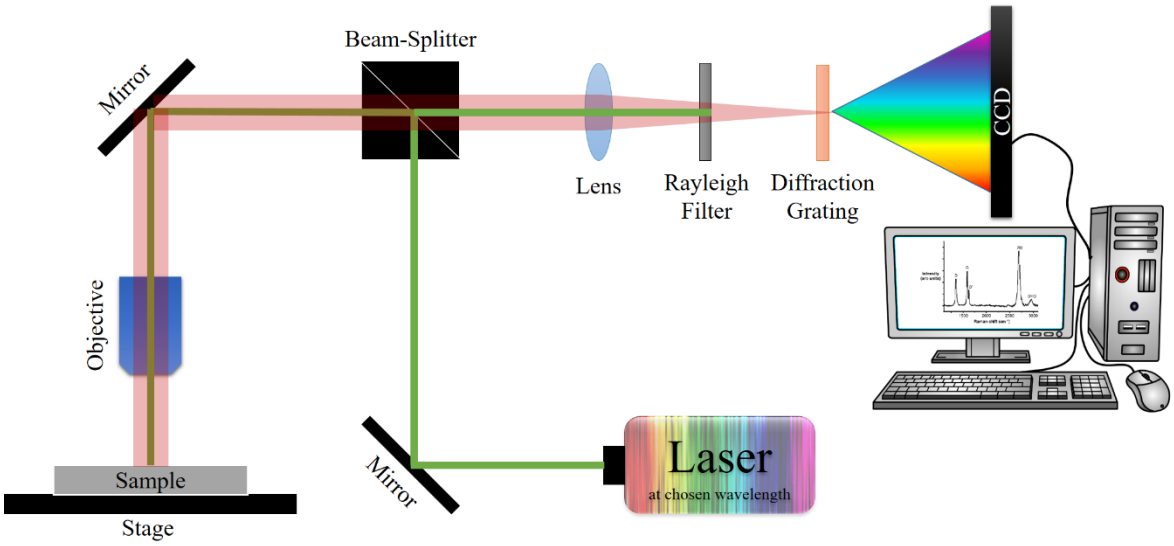

Figure 3.2: Schematic illustration of a Raman microscope

The results of Raman spectroscopy are generally plotted in a two-dimensional graph. The vertical y-axis represents the intensity of received light from photodetectors. At the horizontal x-axis, the Raman shift is given. Raman shift is a variable in wavenumbers, which explains the energy difference between incident light and the light coming from Raman scattering. The relation between Raman shift and corresponding wavelengths is given below, where Raman shift is expressed as $\Delta\tilde{\nu}$, the wavelength of incident light is shown as λ_{ref} and the wavelength of scattered light is expressed as λ_{Rsc}.

$$\Delta\tilde{\nu}\ (cm^{-1}) = 10^7 \left(\frac{1}{\lambda_{\text{ref}}(nm)} - \frac{1}{\lambda_{Rsc}(nm)}\right) \tag{3.1}$$

Characterization of graphene via spectroscopic methods is usually done by Raman spectroscopy. This is sensible since pristine graphene has only carbon-to-carbon molecular bonds, which are centrosymmetric. IR spectroscopy is generally used for identifying

graphene oxide and its derivatives, due to the presence of carbon-to-oxygen bonds (Song et al., 2014).

3.1.2. Raman spectra of graphene and amorphous carbon

For understanding the results of this study better, Raman spectra of pristine and defected graphene along with amorphous carbon must be comprehended. The phonon dispersions of single-layer graphene (SLG) consist of six phonon branches, as three optical (O) and three acoustic (A). (Number of phonon branches = 3N, where N is the number of atoms per unit cell, in this case, "2") Two atoms are present in the unit cell of graphene, so six normal modes, two of which are doubly degenerate, appear at the Brillouin zone center Γ (Reich and Thomsen, 2004). The modes are called "A_{2u}, B_{2g}, $E_{1u,}$ and E_{2g}" respectively. The phonon branches at the Brillouin zone center can be described as "$\Gamma = A_{2u} + B_{2g} + E_{1u} + E_{2g}$". A_{2u} phonon mode is asymmetric with respect to the inversion axis (ungerade), one-dimensional, symmetric with respect to the principal axis, and non-degenerate. B_{2g} phonon mode is symmetric with respect to the inversion axis (gerade), one-dimensional, asymmetric with respect to the principal axis, and non-degenerate. E_{1u} phonon mode is doubly degenerate, two-dimensional, and asymmetric with respect to the inversion axis (ungerade). Finally, E_{2g} phonon mode is doubly degenerate, two-dimensional, and symmetric with respect to the inversion axis (gerade). The gerade modes can be Raman active and among them, only E_{2g} phonon mode is Raman active. B_{2g} phonon mode is neither Raman nor IR active. The high-frequency E_{2g} phonon mode is responsible for the G band, which is visible around 1580 cm^{-1}. The phonon dispersions of graphite are also important since most of the produced graphene is either defective or multi-layered. In the case of graphite, there are 12 phonon branches due to having four atoms per unit cell. Two atoms of the unit cell have four neighbor atoms, which are above or below in adjacent layers; and two atoms of the unit cell are inequivalent. Due to this, the number of optical phonons is doubled and allows IR active bands in graphite. Single-layer graphene optical modes are Davydov-doublets in graphite. Davydov-doublet phonon modes generate another phonon mode along with themselves and this phenomenon leads to doubled phonon modes in total. The phonon modes in graphite can be described as "$\Gamma = 2(A_{2u} + B_{2g} + E_{1u} + E_{2g})$". There are now two doubly degenerate, Raman active E_{2g} modes (Nemanich et al., 1977; Tan, 2012). The D band, which is visible

around 1350 cm^{-1}, is derived from breathing modes of carbon ring and is activated by defects. The D band is not expected to be observed in the center of pristine graphene, but it can be visible at the edges of graphene flakes. In addition, the 2D band is derived from the second-order of zone-boundary phonons. The 2D band, which is visible around 2700 cm^{-1}, is an overtone of the D band. The 2D band originates from a process where momentum is conserved by two phonons with opposite wavevectors, it can be seen in the Raman spectrum of pristine graphene without defects (Ferrari and Basko, 2013). Raman spectra of pristine single-layer graphene and defected graphene are shown in Figure 3.3.

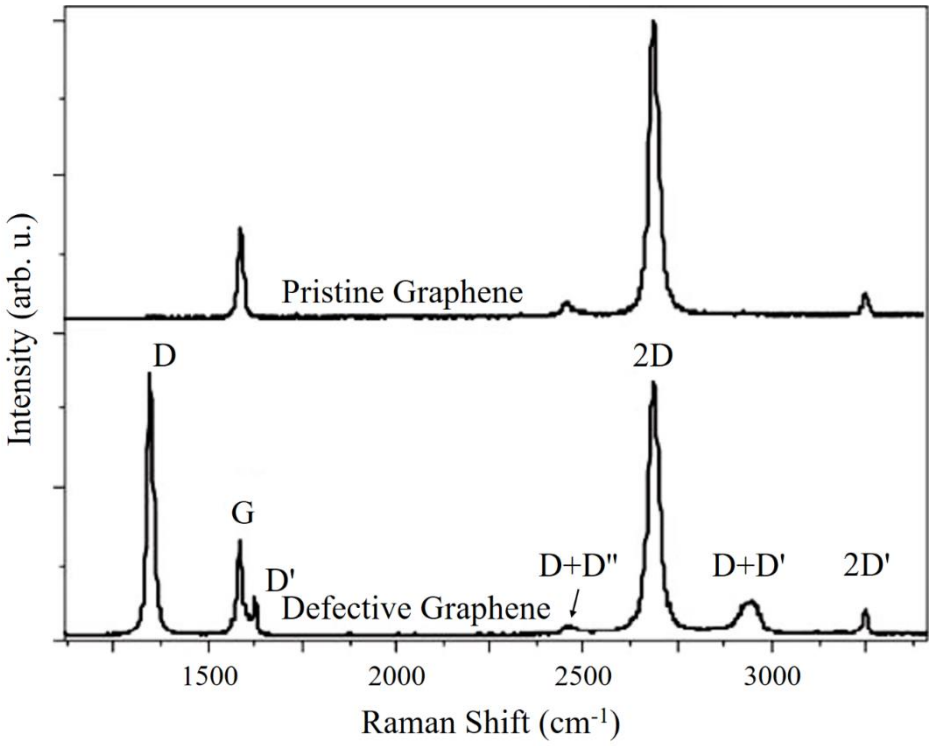

Figure 3.3: Raman spectrum of pristine graphene at the top and Raman spectrum of defected graphene on the bottom with labeled bands (Ferrari and Basko, 2013)

Double resonance can occur in intra-valley processes as well, the D' band, which is visible around 1620 cm^{-1}, is the product of this process. The 2D' band, which is visible around 3250 cm^{-1}, is an overtone band of the D' band. Similarly, the 2D band, the 2D' band requires no defects to be Raman active. The band, which belongs to the longitudinal acoustic branch, seen in defected graphene samples around 1100 cm^{-1}, is called the D'' band. While this band is not visible in Figure 3.3, the peak around 2450 cm^{-1}, is due to the combination

of the D band and the D" band. In addition, the band visible around 2950 cm^{-1} is due to the combination of the D band and the D' band. These bands are important for characterizing graphene samples with Raman spectroscopy.

Raman spectrum of amorphous carbon is also important. While there may be no sharp peaks to identify, the Raman spectrum of amorphous carbon can give information about the ratio of sp^2 and sp^3 bonds present in the sample. The ratio of the intensities of the D band and the G band (I_D/I_G) correlates with the ratio of sp^3 and sp^2 bonds present in the sample (FC and SL, 2006). In addition, the peak of the G band redshifts when there are fewer sp^3 bonds (Kassab et al., 2018). The Raman spectra of various carbon-based materials are given in Figure 3.4.

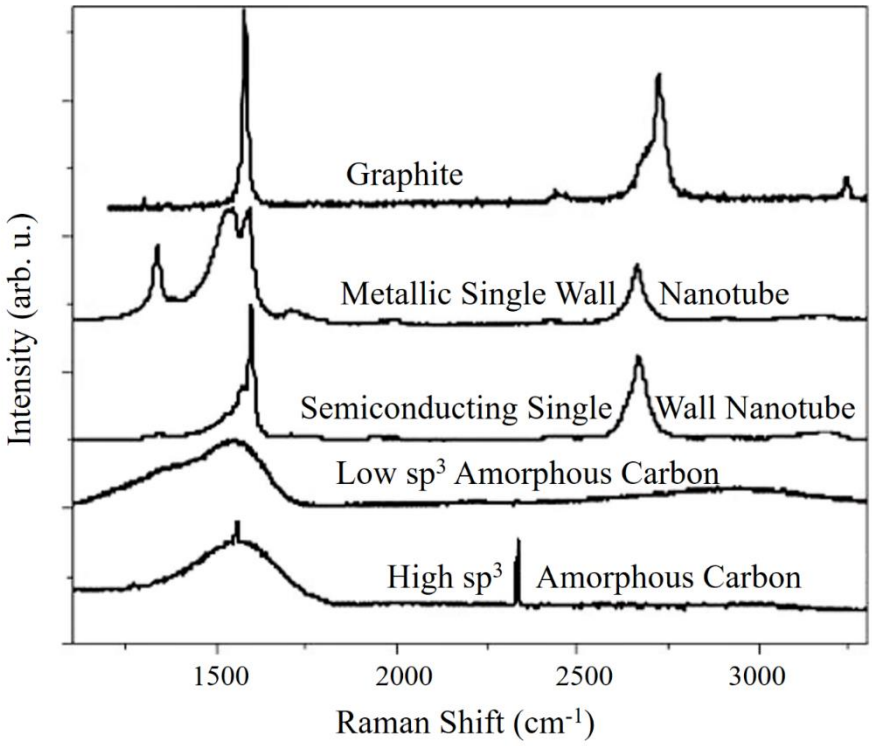

Figure 3.4: Raman spectra of various carbon-based materials (Ferrari and Basko, 2013)

Raman spectra of carbon-based materials are necessary to analyze carbon-based samples, as in our research. The peaks of the bands and their positions with their intensities in the spectrum, give valuable information about the structure of the samples.

3.2. Experimental Method

The basis of the study relies on the findings of previous studies for the investigation of thin films produced by the thermionic vacuum arc technique. In the study of graphene doped tin oxide thin films deposited by thermionic vacuum arc technique, it is found that thin films deposited at room temperature using the TVA method are similar to thin films that were annealed at 600 °C (Demirkol et al., 2019; Choi et al., 1997). This is due to the TVA technique where highly energetic plasma particles are used for deposition. Instead of annealing sample as in CVD methods, energetic particles are presented to the system to catalyze sp^3 bonds into sp^2 bonds thus expecting to form graphene. Since all the process occurs at room temperature and being a physical vapor deposition method, TVA technique could integrate into processes for producing semiconductor devices.

3.2.1. Thermionic vacuum arc technique

The thermionic vacuum arc technique is a deposition method, where electrons are released into a vacuum chamber using a tungsten filament and accelerated onto deposition material, which turns into plasma deposited onto a substrate in a high vacuum environment. Deposition material can be in solid, liquid, and gaseous form (Pat et al., 2014). Additionally, various materials can be mixed during the deposition process, enabling different structures to be formed. The basic scheme of TVA is illustrated in Figure 3.5.

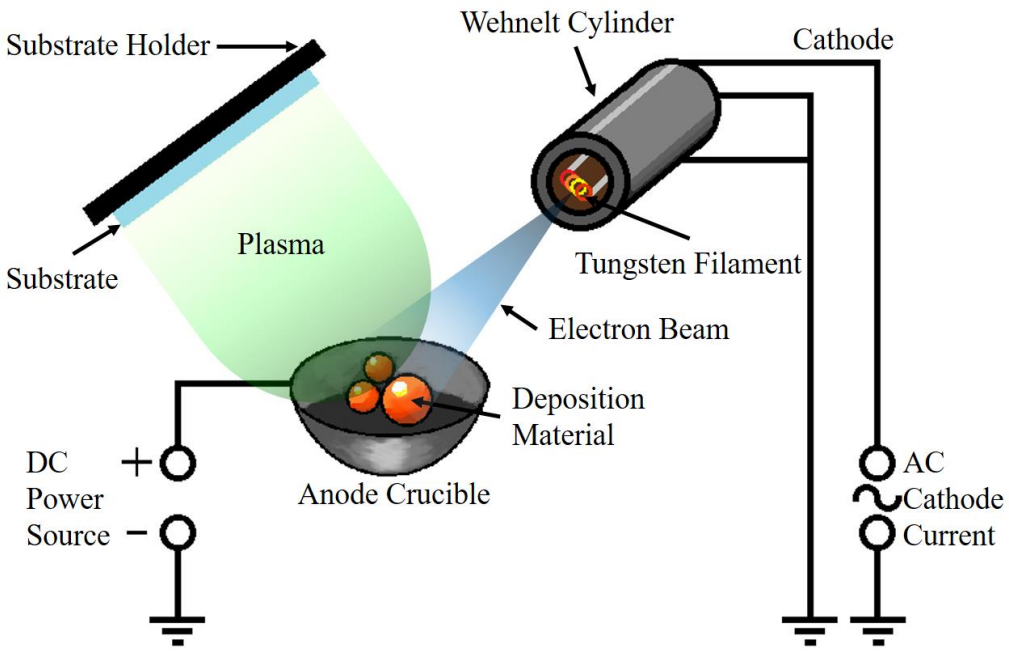

Figure 3.5: The basic scheme of thermionic vacuum arc

AC current is applied to tungsten filament to create thermionic emission. Free electrons are directed onto deposition material by using an external DC power source and grounded Wehnelt cylinder. Electrons are accelerated towards anode crucible, which holds deposition material, by applying positive potential difference. While deposition material is being bombarded with electrons, evaporates into plasma if the potential difference is sufficient. The particles in plasma are highly energetic. The plasma obtained is deposited onto a substrate, where it forms a thin film structure.

The TVA technique must be applied within a vacuum chamber in a high vacuum (Pressure ~10^{-6} torr). This necessity is due to two main factors. If AC current flows through tungsten filament in oxygen presence, it would oxidize rapidly and burn out. Secondly, if the vacuum is not high enough, the electron beam would fluctuate and could make an arc into places other than anode crucible. In addition, a high vacuum environment helps to create homogenous thin films with low impurities. Various materials, such as metals, ceramics, and semiconductors, can be deposited using the TVA technique. Since the process occurs at room

temperature and provides good adhesiveness, different materials can be used as substrates, even the ones that are hard to coat such as stainless steel (Dinca et al., 2020).

3.2.2. Sample preparation

The basic structure of our research has multiple steps. Firstly, soda-lime glass microscope slides are cleaned with ethanol and deionized (DI) water and prepared for use as substrates. The prepared substrates are placed into the vacuum chamber for the deposition process. ISOLAB microscope slides were used. Secondly, the first deposition process takes place. In the first deposition process, either activated carbon or desired transition metals are used as deposition material. After this step, the second deposition process is carried out. For the second deposition process, the selected deposition material is either activated carbon or transition metals. If carbon is deposited onto the substrate in the first process, the deposition material would be transition metals and vice versa. After both depositions, the transition metal layer is etched with a ferric acid solution. After rinsing the samples with deionized water, the samples are investigated with Raman spectroscopy. The basic structure of the research is shown in Figure 3.6.

It is also worth mentioning that three different substrates were tested at the beginning. Along with soda-lime glass microscope slides, phosphorus-doped n-type silicon wafers and PVC sheets were tested. Using silicon wafers and PVC sheets as substrates were abandoned. Due to the number of samples produced, using silicon wafers was too costly. Also, the adhesiveness of the carbon layer to the silicon surface was weak and all layers of most samples produced onto silicon substrate were completely removed after etching with ferric chloride solution. PVC is a material, consists of carbon, hydrogen, and chlorine atoms. Due to the presence of carbon bonds, the Raman spectrum of PVC includes numerous peaks, which overlap with the bands present in the Raman spectrum of graphene. For these reasons, silicon wafers and PVC sheets were not used as substrates in this study.

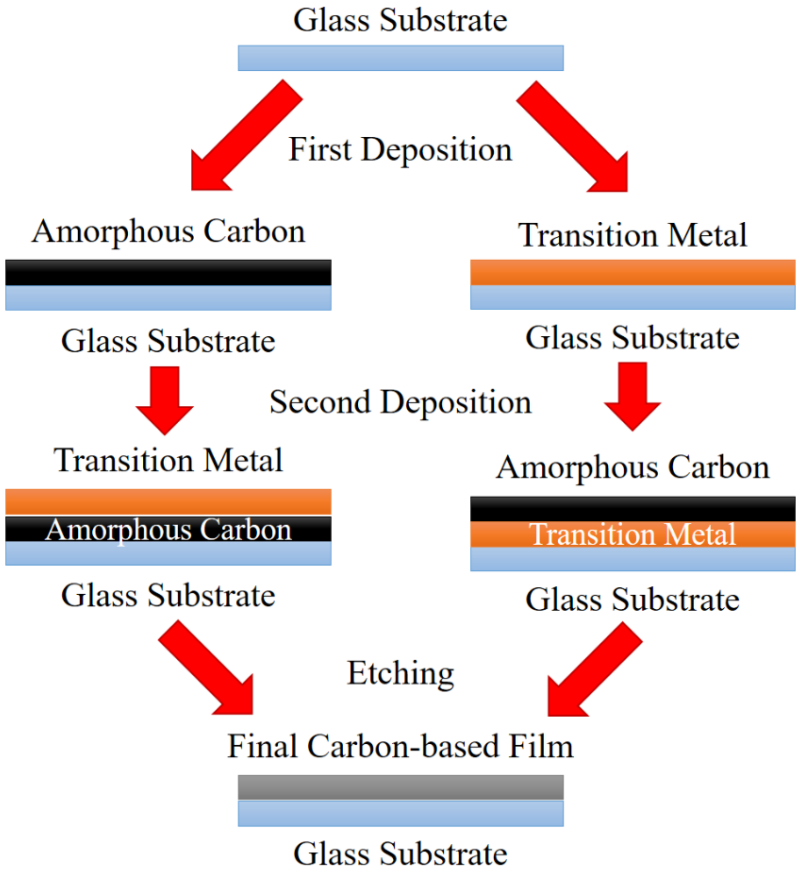

Figure 3.6: The schematic representation of the sample preparation

4. RESULTS AND DISCUSSION

In the course of this study, more than fifty samples were prepared, more than a hundred deposition processes were conducted, and more than two hundred Raman spectroscopies were investigated. Every deposition process along with sample preparation takes about two hours. In addition to this tremendous effort, every step had its own difficulties. This is due to the nature of this study. New methods and tools were needed to conduct new unprecedented experiments continuously. The trickiest part was the deposition of nickel. It took about a month to explore experimental parameters and form a recipe, along with know-hows. In this thesis, the most defining results will be shared. This is due to two major reasons. Firstly, not all samples were prepared as it was desired. There were many trials and errors in the course of this study. Even though these samples were investigated with the Raman microscope, but there were not any noteworthy results. Secondly, the results from the same approaches were quite similar. This is also indicating the homogeneity of our samples.

In this study, various approaches have been investigated and the samples were produced accordingly. Produced samples were investigated using Raman spectroscopy. Raman spectroscopy was conducted with Renishaw inVia Raman Microscope. The Raman spectra of the samples will be discussed similarly to the sequence of our research's progress.

4.1. Raman Spectrum of Carbon Thin Film on a Glass Substrate

For understanding the progress in this study, the Raman spectrum of carbon thin film on glass substrate must be investigated. This is necessary since it will be the reference point for further investigations. The carbon thin film was deposited using the TVA technique. The filament current was 20.5 A and the applied voltage was 200 V. There was no discharge current during deposition, and the substrate was coated with sublimed activated carbon gas. The deposition took a minute and was performed at 9.1×10^{-5} torr pressure. The sample was investigated with a Raman microscope using a 532 nm laser and a 100x magnification

objective lens. The Raman spectrum of carbon thin film deposited onto a glass substrate is presented in Figure 4.1.

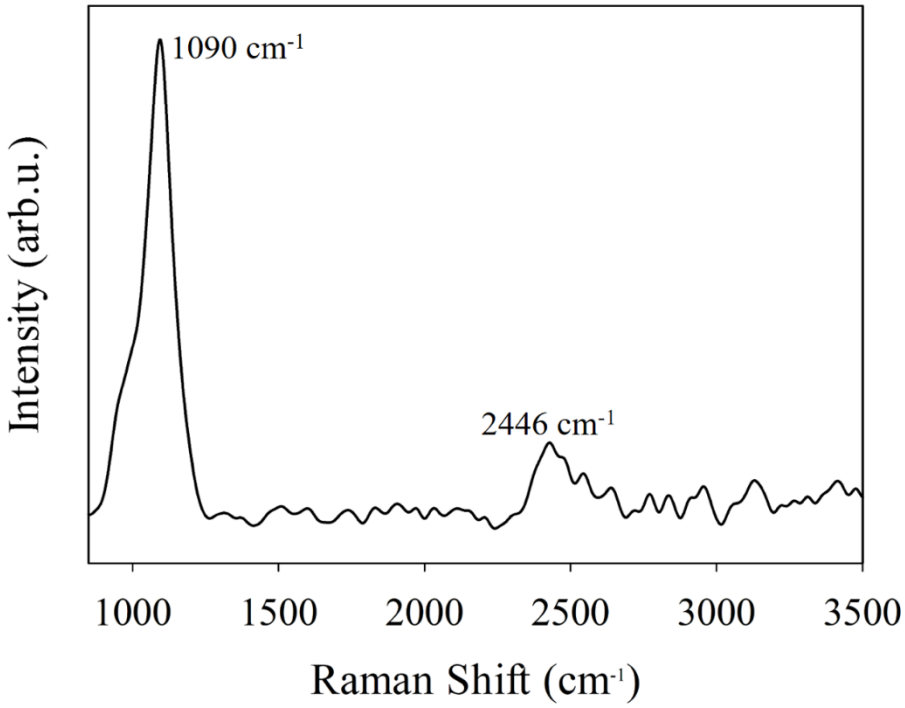

Figure 4.1: The Raman spectrum of carbon thin film deposited with TVA technique on a glass substrate

There are two prominent peaks in the Raman spectrum of carbon thin film, deposited with the TVA technique. The first peak visible at 1090 cm^{-1}, is mainly derived from soda-lime glass, with the possibility of an insignificant amount coming from the D" band, which is around 1100 cm^{-1} (Redkov et al., 2019). Similarly, the second peak is mainly obtained from soda-lime glass, with the possibility of an insignificant amount coming from the D + D" band, which is around 2450 cm^{-1}. The contribution from the D" band is highly unlikely since the D band is nearly invisible. The lack of carbon-related peaks in the spectrum is possible if the thin film is too thin and too disordered, thus the signal from carbon-related peaks cannot be separated from the noise coming from the substrate.

4.2. First Approach

At the beginning of our study, our approach was mainly inspired by graphene synthesis on copper with the CVD method. Since achieving monolayer graphene flakes were aimed at the beginning, copper was used for catalyzing carbon bonds, hoping to find similar results as CVD on copper. In this approach, firstly copper was deposited onto a glass substrate using the TVA method. The filament current was 18.5 A and the applied voltage was 400 V. The discharge current during deposition was 0.4 A. The deposition took 90 seconds and was performed at $1.2x10^{-4}$ torr pressure. After the deposition of copper, the tungsten crucible used for copper deposition was changed with the tungsten crucible used for carbon specifically. The TVA technique was used for the deposition of carbon as well. The parameters for the deposition of carbon were similar to the previously mentioned carbon deposition parameters. After both depositions, the copper layer of a sample was tried to be removed with ferric chloride solution. During this etching process, all thin films deposited were removed from the surface and there were flake-like floating thin film pieces in the solution. Those pieces were suspected to be from the carbon layer, which is insoluble within ferric chloride solution. The other samples were investigated with the Raman microscope using a 532 nm laser and a 100x magnification objective lens. The Raman spectrum of the sample made of carbon/copper/glass, from top to bottom, is presented in Figure 4.2.

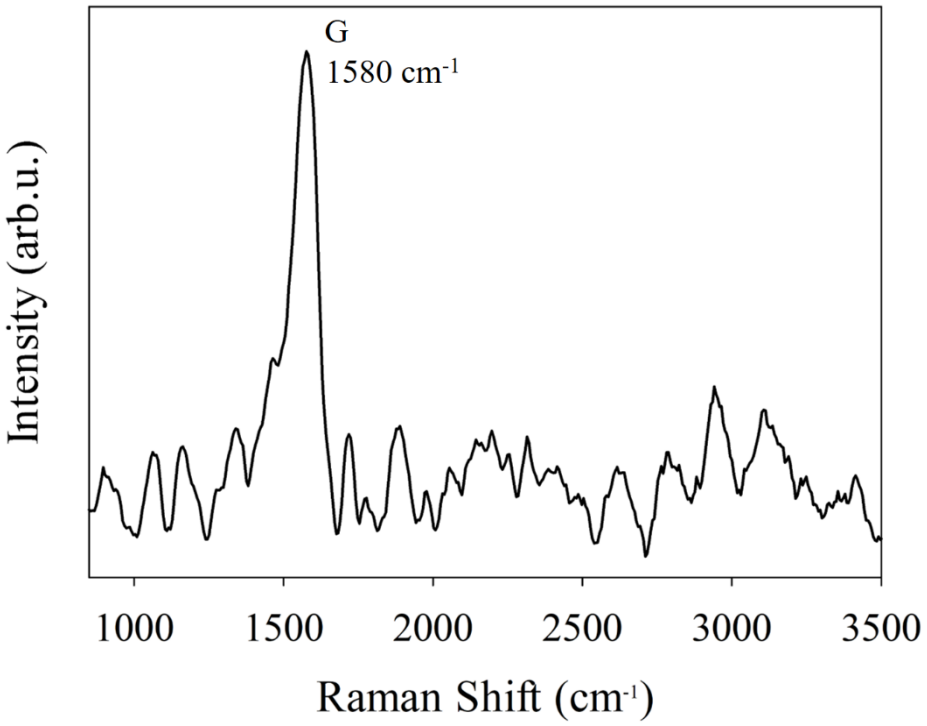

Figure 4.2: The Raman spectrum of the sample made of carbon/copper/glass with TVA technique

The only noticeable peak in the spectrum is the G band at 1580 cm^{-1}. While the G band signal was weak, the addition of a copper layer, a transition metal layer, was able to create some sp^2 bonds. There were some complications regarding this approach. Firstly, the copper layer was removed along with the carbon layer. This would be avoidable with using a copper foil substrate and transferring the carbon layer onto another substrate, but this would not fit into our goal of synthesizing graphene with a method, which is applicable to the manufacturing processes of semiconductor devices. Secondly, the results were not satisfactory, but it was the first sign of the catalysis process needed for synthesizing graphene.

4.3. Second Approach

The next attempt was focused on keeping the carbon layer on the substrate after the etching process, and to achieve that, onto a glass substrate carbon was selected as the first layer to deposit, and copper was selected as the second layer to deposit. In addition, in the

first approach, the carbon was deposited onto the copper layer at room temperature. With this approach, the amount of energy transferred to carbon atoms would be higher with the plasma of copper. The parameters of the TVA setup were similar to the ones before. After both depositions, the copper layers of all samples were etched with ferric chloride solution. The samples were investigated with a Raman microscope using a 532 nm laser and a 100x magnification objective lens. The Raman spectrum of carbon thin films in the second approach is given in Figure 4.3.

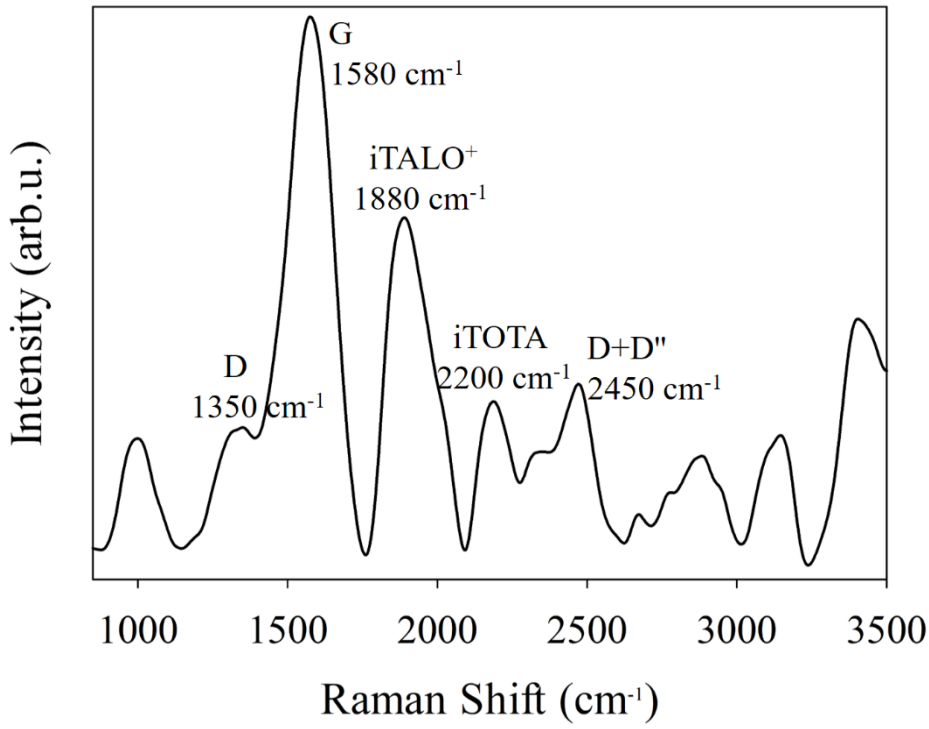

Figure 4.3: The Raman spectrum of the sample made of copper/carbon/glass with TVA technique, after copper layer etched

The peaks observed in the spectrum were very weak and very hard to separate from background noise. Even though, there was enough intensity to identify few peaks. The G band is clearly visible. The presence of the G band shows there are sp^2 bonds formed. Additionally, the D band, which hints at sp^3 bonds, is slightly visible in the spectrum. The combination of the D band and the D" band is also somewhat visible. Surprisingly, there are two identified unexpected but probable peaks. The first one ($iTALO^+$) is the peak at 1880 cm^{-1} in the spectrum. This band derives from the combination of the out-of-plane transverse

optical and longitudinal optical (oTO + LO) phonons branches around the K point in the Brillouin zone of graphene. The second peak (iTOTA) is the one at 2200 cm^{-1} in the spectrum. This peak comes from the combination of in-plane transverse optical (iTO) and in-plane transverse acoustic (iTA) phonons around the K point. These peaks were detected from single-layer graphene on silicon dioxide substrate in the literature (Rao et al., 2011). The chosen names for these bands are taken from the reference study of Rao and his co-workers.

4.4. Third Approach

The last two approaches were not ideal due to the annealing temperature of copper is relatively high and the potential difference required for the transition of copper into plasma state is relatively low. This conclusion is derived from the relatively weak Raman peaks. Copper had been deposited onto carbon film for one approach and copper had been deposited under carbon film for another approach. Both approaches with copper yielded unsuccessful for obtaining graphene flakes. These results changed our focus to other transition metals and nickel was chosen due to having high carbon solubility inside and annealing temperature of nickel is relatively low and the potential difference required for the transition of nickel into plasma state is relatively high (Hu et al., 2015). There is a single issue with using nickel. Nickel forms an alloy with tungsten rapidly and lowers the melting point of each metal below its pure melting points (Skoczylas et al., 2020). Since the crucible used is made of tungsten, big chunks of nickel are used as deposition material and the electron beam is directed to a small pocket on the nickel to avoid forming a nickel-tungsten alloy.

The next approach was based on the deposition of nickel onto a carbon layer on a glass substrate. The deposition of the nickel layer took place at $7.5x10^{-5}$ torr pressure, with a filament current of 20.5 A and 700 V of applied voltage in 90 seconds. The discharge current was 0.4 A. After the deposition of both layers, the nickel layer was etched in ferric chloride solution. The samples were investigated with the Raman microscope using a 532 nm laser and a 100x magnification objective lens. The Raman spectrum of the sample made of nickel/carbon/glass is shown in Figure 4.4.

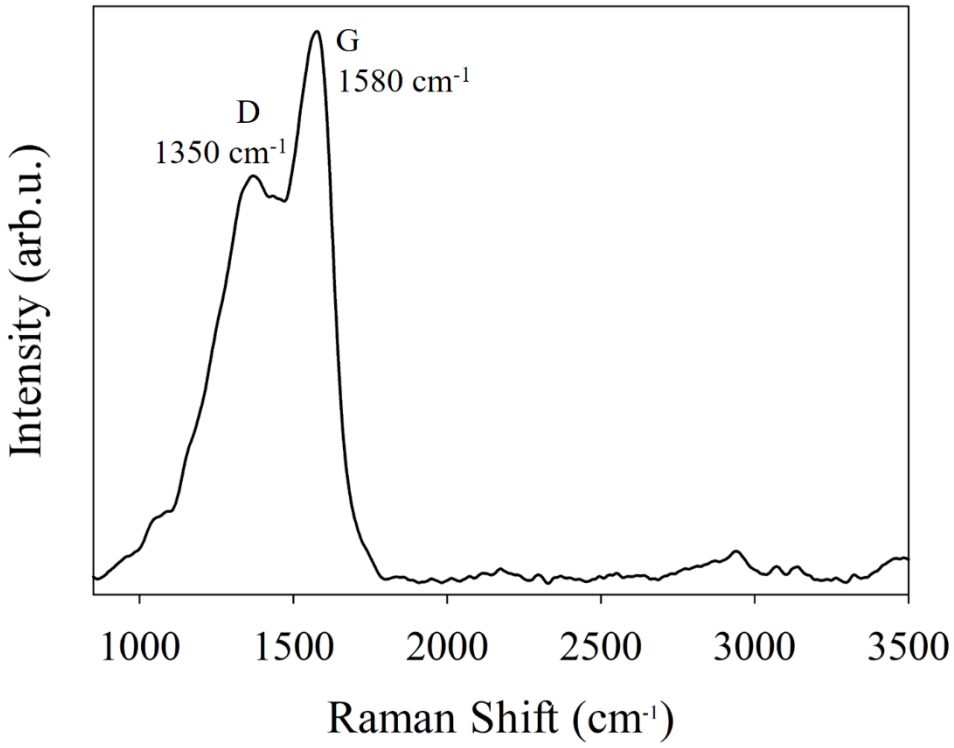

Figure 4.4: The Raman spectrum of the sample made of nickel/carbon/glass with TVA technique, after nickel layer etched

The results from the Raman spectrum of this approach were promising. The peaks in the spectrum were very clear and easy to separate from background noise. This led to accurately calculate the ratio of I_D/I_G, which is calculated as 0.87. Additionally, the 2D band was not observed. If the edges of graphitic materials are terminated or graphitic layers are stacked disorderly, the 2D band can diffuse and not be visible in the spectrum (Villa and Dimitratos, 2018; Groppo et al., 2018; Alrefae et al. 2017). The ratio of I_D/I_G is more informative about the quality of graphitic materials. It was clear that the samples produced with this approach are more graphene-like and it is more feasible to focus on and enhance this approach.

4.5. Last Approach

In all approaches experimented, one issue was certain. The deposition of the transition metal layer catalyzed sp^3 bonds into sp^2 bonds to a certain extent. In our previous approaches, the desired ratio of sp^2 bonds could not be reached. For this reason, it was

necessary to put forward a new approach suitable for our target and possibilities. The process got better with each trial, but getting the results wanted required a new approach. In order to increase the sp^2 bond ratio, it was decided to repeat the nickel deposition process on the carbon layer and the nickel deposition process was repeated three times. After each time the nickel layer was etched with ferric chloride solution. The samples were investigated with a Raman microscope using a 532 nm laser and a 100x magnification objective lens. The Raman spectrum of the sample made of nickel/carbon/glass, after nickel layer, three times both deposited and etched, is given in Figure 4.5.

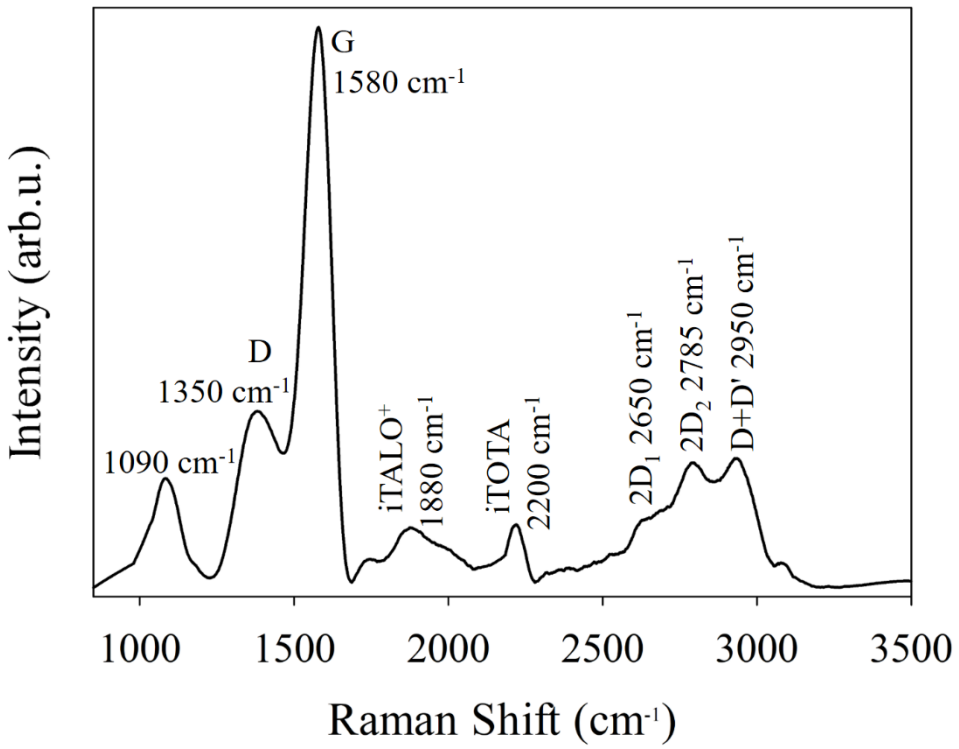

Figure 4.5: The Raman spectrum of the sample made of nickel/carbon/glass, after nickel layer, three times both deposited and etched

This is the best result achieved in this study. The Raman spectrum was relatively noise-free, compared to other spectra in this study. Along with the G and D bands, the 2D band is also visible, while widened and split. The ratio of I_D/I_G was calculated as 0.32. This means that in the last approach, the ratio of sp^2 bonds has been increased. This also proves our suggestion, which was repeating the deposition of the nickel layer could increase the sp^2 bonds present in the sample. However, the peaks are still wider than the ones present in the

Raman spectra of pristine graphene and graphite. This indicates the presence of amorphous bond structures. Due to the presence of the 2D bands, the ratio of I_G/I_{2D} could be calculated as 4.51. There could be several reasons for the diffusion of the 2D band, as well as the multilayer nature of the sample. For that reason, the number of graphene layers present in the sample is undefined.

4.6. General Overview

The progress achieved during this study is reflected in the Raman spectra of the samples. In order to see this progress in perspective, all Raman spectra of the samples were combined in Figure 4.6, where the Carbon/Glass spectrum represents the sample of a carbon layer onto a glass substrate without any transition metal layer deposited; Carbon/Copper/Glass spectrum represents the sample made of a carbon layer on top of a copper layer onto a glass substrate; Copper/Carbon/Glass spectrum represents the sample made of copper layer on top of carbon layer onto a glass substrate, but the copper layer is etched; Nickel/Carbon/Glass spectrum represents the sample made of nickel layer on top of carbon layer onto a glass substrate, but nickel layer is etched, and finally 3x Nickel/Carbon/Glass spectrum represents the sample made of nickel layer on top of carbon layer onto a glass substrate, but three times both deposited and etched.

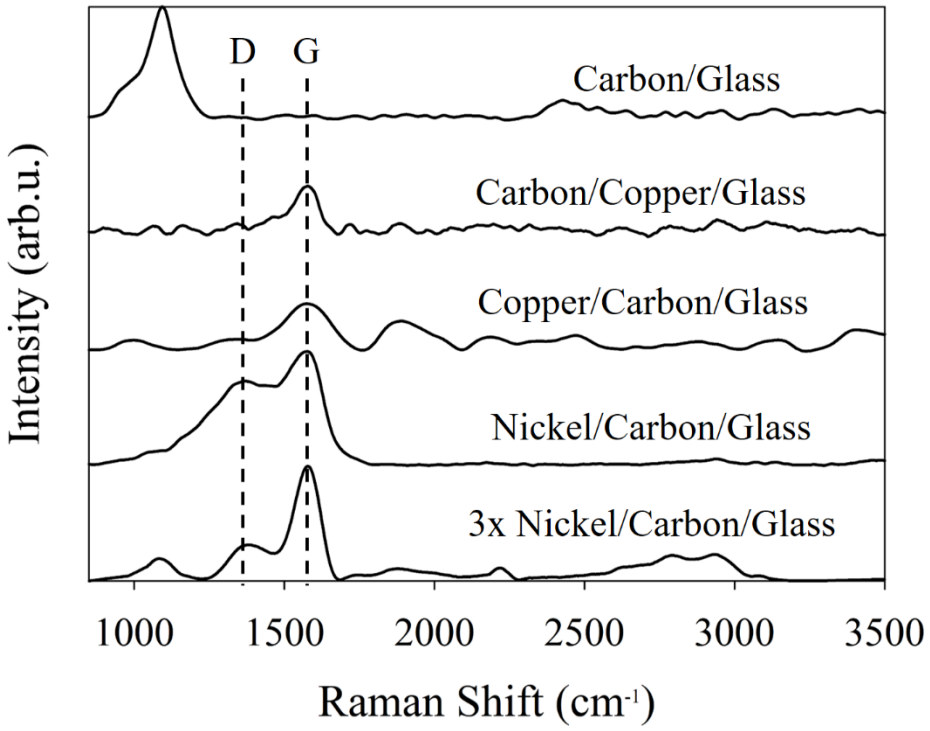

Figure 4.6: The normalized Raman spectra of the samples that represent each approach

While the intensities in the spectra are arbitrary and cannot be compared with one another between different spectra, the decrease in the ratio of I_D/I_G, noise and width of the G band can be seen in Figure 4.6.

5. CONCLUSIONS AND RECOMMENDATIONS

The aim of this study was to synthesize graphene with a physical vapor deposition method at room temperature onto any substrate, to create a method, which is integrable to the semiconductor device manufacturing process. The thermionic vacuum arc technique was utilized to achieve this goal since the materials deposited with the TVA technique are highly energetic during the deposition process and have the potential to negate the need for high-temperature processes. The objectives of this study were met in an improvable way.

In the first approach of this study, with the TVA technique, the copper layer was deposited onto a glass substrate, and then the carbon layer was deposited on top of them. The samples created with this approach were investigated with a Raman microscope using a 532 nm laser and a 100x magnification objective lens. The only noticeable peak was the G band at 1580 cm^{-1}, which was not present at the spectrum of the sample made of a carbon layer onto a glass substrate without any transition metal layer deposited. The noise in the spectrum was quite noticeable. These results indicate the catalysis of amorphous carbon into graphitic material with the help of a transition metal layer at near room temperature. The copper layer could not be removed without removing the carbon layer. For this reason, this approach was not suitable for the goals of this study.

In the second approach of this study, the carbon layer was deposited onto a glass substrate, then the copper layer was deposited on top of the whole sample with the TVA technique. In this approach, the copper layer was able to be etched in a ferric chloride solution, without removing or damaging the carbon layer. The samples were investigated with a Raman microscope using a 532 nm laser and a 100x magnification objective lens. The Raman spectrum was very hard to separate from background noise. Nonetheless, the spectrum showed the G band at 1580 cm^{-1}, the D band at 1350 cm^{-1}, and the combination of the D band and the D" band at 2450 cm^{-1}. Additionally, two bands that are present in the spectrum of single-layer pristine graphene on silicon dioxide substrate, the $iTOLA^{+}$ at 1880 cm^{-1} and the iTALO at 2200 cm^{-1}, were also present in the spectrum. Despite the numerous peaks available at the Raman spectrum, the high ratio of the background noise to signal hints that the catalysis of the carbon layer into a graphitic material is limited. However, the carbon

layer was not removed along with the copper layer in the etching process and this approach was a step in the right direction to achieve the goal of this study.

In the third approach experimented, using the TVA technique, the carbon layer was deposited onto a glass substrate, then instead of using copper as a transition metal, nickel was used and the nickel layer deposited on top of the whole sample. After both depositions, the nickel layer was etched with a ferric chloride solution and the Raman spectra of the samples were obtained with a Raman microscope using a 532 nm laser and a 100x magnification objective lens. The peaks acquired from the Raman spectrum were the D band at 1350 cm^{-1} and the G band at 1580 cm^{-1}. The peaks were overlapped into each other, similarly to the Raman spectrum of an amorphous carbon sample. However, the intensities of the peaks were strong and the peaks were able to easily separated from the background noise. Using nickel as a transition metal helped to catalyze the sp^3 bonds present in the sample into the sp^2 bonds, more than copper. The ratio of I_D/I_G was calculated as 0.87, which indicates the catalysis process had not been fully completed.

In the last approach experimented, which is similar to the third approach with the exception of the number of times that the nickel layer deposited and etched, the nickel layer of the samples were both deposited and etched three times, before the samples were investigated with a Raman microscope using a 532 nm laser and a 100x magnification objective lens. The reason for this repetition was to increase the number of the sp^2 bonds, relative to the sp^3 bonds. The Raman spectrum showed the presence of the D band at 1350 cm^{-1}, the G band at 1580 cm^{-1}, the iTALO$^+$ band at 1880 cm^{-1}, the iTOTA band at 2200 cm^{-1}, and the combination of the D band and the D' band at 2950 cm^{-1}. Additionally to these bands, the 2D band was present in the spectrum, while being split into two peaks as the $2D_1$ band at 2650 cm^{-1} and the $2D_2$ band at 2785 cm^{-1}. The Raman spectrum of the samples produced with the last approach shows similarity to the Raman spectrum of a multilayer graphene sample. The ratio of I_D/I_G was calculated as 0.32, which is lower than the ratio from the previous approach and shows the effective catalysis process. Additionally, the ratio of I_G/I_{2D} was calculated as 4.51. The ratio of I_G/I_{2D} is generally used for the determination of the number of graphene layers present in a sample, but since glass microscope slides were used as substrates, the intensity of the 2D band can be misleading. However, even the

presence of the 2D band indicates graphene flakes forming in the sample. In addition, the overlapping sections of the peaks of the G band and D band are greatly reduced, and the peak profiles were sharpened relative to previous approaches. Nonetheless, there are still some overlapping sections present and the peak profiles are not sharp as pristine graphene samples. This broadening in the peaks hints amorphous bond structures are still present in the sample.

The goal of synthesizing graphene flakes with a physical vapor deposition method at room temperature was achieved. However, the quality of the samples is arguable. There might be few actions to increase the quality. The carbon layer might be annealed in an atmosphere of 100% hydrogen gas, to terminate carbon bonds, later to be catalyzed by a transition metal layer more easily. This process can be studied at varying temperatures. In addition, the samples produced can be annealed in an oxygen-free environment without any etching process beforehand, and thermal analysis of the samples can be done to observe the ideal temperature point for maximum catalysis. The different transition metals can be used for the catalysis of carbon. However, most of these suggestions require annealing of the sample at one point, which is undesirable for the goal of this study.

It is also worth mentioning that further studies can be conducted to obtain other physical properties of the graphene samples obtained with the methods in our study. Some devices or structures can be made with the graphene obtained with the TVA technique to test the electronic and mechanical properties of the graphene used compared to the graphene produced with other established methods.

Overall, this study tackled big questions and created a guideline for further studies. While there is room for improvement, it is shown that physical vapor deposition methods can be alternative to other synthesis methods of graphene.

REFERENCES

Abbandanak, S. H., Aghamohammadi, H., Akbarzadeh, E., Shabani, N., Eslami-Farsani, R., Kangooie, M., & Siadati, M. H. (2019). Morphological/SAXS/WAXS studies on the electrochemical synthesis of graphene nanoplatelets. *Ceramics International*, *45*(16), 20882-20890.

Alofi, A., & Srivastava, G. P. (2013). Thermal conductivity of graphene and graphite. *Physical Review B*, *87*(11), 115421.

Alrefae, M. A., Kumar, A., Pandita, P., Candadai, A., Bilionis, I., & Fisher, T. S. (2017). Process optimization of graphene growth in a roll-to-roll plasma CVD system. *AIP Advances*, *7*(11), 115102.

Amarnath, C. A., Hong, C. E., Kim, N. H., Ku, B. C., Kuila, T., & Lee, J. H. (2011). Efficient synthesis of graphene sheets using pyrrole as a reducing agent. *Carbon*, *49*(11), 3497-3502.

Bernath, P. F. (2020). *Spectra of atoms and molecules*. Oxford university press.

Bhuyan, M. S. A., Uddin, M. N., Islam, M. M., Bipasha, F. A., & Hossain, S. S. (2016). Synthesis of graphene. *International Nano Letters*, *6*(2), 65-83.

Brodie, B. C. (1859). XIII. On the atomic weight of graphite. *Philosophical transactions of the Royal Society of London*, (149), 249-259.

Cao, Y., Fatemi, V., Fang, S., Watanabe, K., Taniguchi, T., Kaxiras, E., & Jarillo-Herrero, P. (2018). Unconventional superconductivity in magic-angle graphene superlattices. *Nature*, *556*(7699), 43-50.

Chae, S. J., Güneş, F., Kim, K. K., Kim, E. S., Han, G. H., Kim, S. M., ... & Lee, Y. H. (2009). Synthesis of large-area graphene layers on poly-nickel substrate by chemical vapor deposition: wrinkle formation. *Advanced materials*, *21*(22), 2328-2333.

Chang, I. L., & Chen, J. A. (2015). The molecular mechanics study on mechanical properties of graphene and graphite. *Applied Physics A*, *119*(1), 265-274.

Chen, Z., Lin, Y. M., Rooks, M. J., & Avouris, P. (2007). Graphene nano-ribbon electronics. *Physica E: Low-dimensional Systems and Nanostructures*, *40*(2), 228-232.

Choi, W. K., Sung, H., Kim, K. H., Cho, J. S., Choi, S. C., Jung, H. J., ... & Jeong, K. (1997). Oxidation process from SnO to SnO 2. *Journal of materials science letters*, *16*(19), 1551-1554.

Choucair, M., Thordarson, P., & Stride, J. A. (2009). Gram-scale production of graphene based on solvothermal synthesis and sonication. *Nature nanotechnology*, *4*(1), 30.

Coraux, J., N 'Diaye, A. T., Busse, C., & Michely, T. (2008). Structural coherency of graphene on Ir (111). *Nano letters*, *8*(2), 565-570.

De Heer, W. A., Berger, C., Wu, X., First, P. N., Conrad, E. H., Li, X., ... & Martinez, G. (2007). Epitaxial graphene. *Solid State Communications*, *143*(1-2), 92-100.

REFERENCES (Continued)

Deacon, R. S., Chuang, K. C., Nicholas, R. J., Novoselov, K. S., & Geim, A. K. (2007). Cyclotron resonance study of the electron and hole velocity in graphene monolayers. *Physical Review B*, *76*(8), 081406.

Delhaes, P. (Ed.). (2000). *Graphite and precursors* (Vol. 1). CRC Press.

Demirkol, U., Pat, S., Mohammadigharehbagh, R., Musaoğlu, C., Özgür, M., Elmas, S., ... & Korkmaz, Ş. (2019). Determination of the structural, morphological and optical properties of graphene doped SnO thin films deposited by using thermionic vacuum arc technique. *Physica B: Condensed Matter*, *569*, 14-19.

Dikin, D. A., Stankovich, S., Zimney, E. J., Piner, R. D., Dommett, G. H., Evmenenko, G., ... & Ruoff, R. S. (2007). Preparation and characterization of graphene oxide paper. *Nature*, *448*(7152), 457-460.

Dinadayalane, T. C., & Leszczynski, J. (2010). Remarkable diversity of carbon–carbon bonds: structures and properties of fullerenes, carbon nanotubes, and graphene. *Structural Chemistry*, *21*(6), 1155-1169.

Dinca, P., Butoi, B., Lungu, M., Porosnicu, C., Jepu, I., Staicu, C., ... & Soreanu, G. (2020). Antibacterial efficiency of stainless-steel grids coated with Cu-Ag by thermionic vacuum arc method. *Coatings*, *10*(4), 322.

Dutta, A. K. (1953). Electrical conductivity of single crystals of graphite. *Physical Review*, *90*(2), 187.

Eizenberg, M., & Blakely, J. M. (1979). Carbon interaction with nickel surfaces: Monolayer formation and structural stability. *The Journal of Chemical Physics*, *71*(8), 3467-3477.

Eizenberg, M., & Blakely, J. M. (1979). Carbon monolayer phase condensation on Ni (111). *Surface Science*, *82*(1), 228-236.

Fan, X., Peng, W., Li, Y., Li, X., Wang, S., Zhang, G., & Zhang, F. (2008). Deoxygenation of exfoliated graphite oxide under alkaline conditions: a green route to graphene preparation. *Advanced Materials*, *20*(23), 4490-4493.

FC, T., & SL, T. (2006). Correlation between ID⁄ IG ratio from visible raman spectra and sp2/sp3 ratio from XPS spectra of annealed hydrogenated DLC film. *Materials transactions*, *47*(7), 1847-1852.

Ferrari, A. C., & Basko, D. M. (2013). Raman spectroscopy as a versatile tool for studying the properties of graphene. *Nature nanotechnology*, *8*(4), 235-246.

Ferrari, A. C., Meyer, J. C., Scardaci, V., Casiraghi, C., Lazzeri, M., Mauri, F., ... & Geim, A. K. (2006). Raman spectrum of graphene and graphene layers. *Physical review letters*, *97*(18), 187401.

Fujita, M., Wakabayashi, K., Nakada, K., & Kusakabe, K. (1996). Peculiar localized state at zigzag graphite edge. *Journal of the Physical Society of Japan*, *65*(7), 1920-1923.

Gall, N. R., Rut'Kov, E. V., & Tontegode, A. Y. (2000). Intercalation of nickel atoms under two-dimensional graphene film on (111) Ir. *Carbon*, *38*(5), 663-667.

REFERENCES (Continued)

Garlow, J. A., Barrett, L. K., Wu, L., Kisslinger, K., Zhu, Y., & Pulecio, J. F. (2016). Large-area growth of turbostratic graphene on Ni (111) via physical vapor deposition. *Scientific reports*, *6*(1), 1-11.

Geim, A. K., & Novoselov, K. S. (2010). The rise of graphene. In *Nanoscience and technology: a collection of reviews from nature journals* (pp. 11-19).

Groppo, E., Bonino, F., Cesano, F., Damin, A., & Manzoli, M. (2018). Raman, IR and INS characterization of functionalized carbon materials.

Hasan, M. Z., & Kane, C. L. (2010). Colloquium: topological insulators. *Reviews of modern physics*, *82*(4), 3045.

Hecht, J. (1989). Physical Limits of Computing: How close has semiconductor technology come to the limits imposed by fundamental physics?. *Computers in Physics*, *3*(4), 34-40.

Hirsch, A. (2010). The era of carbon allotropes. *Nature materials*, *9*(11), 868-871.

Hu, X., Björkman, T., Lipsanen, H., Sun, L., & Krasheninnikov, A. V. (2015). Solubility of boron, carbon, and nitrogen in transition metals: getting insight into trends from first-principles calculations. *The Journal of Physical Chemistry Letters*, *6*(16), 3263-3268.

Hummers Jr, W. S., & Offeman, R. E. (1958). Preparation of graphitic oxide. *Journal of the american chemical society*, *80*(6), 1339-1339.

Karu, A. E., & Beer, M. (1966). Pyrolytic formation of highly crystalline graphite films. *Journal of Applied Physics*, *37*(5), 2179-2181.

Kassab, L. R. P., Santos, A. D. D., & Pillis, M. F. (2018). Evaluation of carbon thin films using Raman spectroscopy. *Materials Research*, *21*(4).

Keiter, R. L. (1983). Spectroscopically silent fundamental vibrations. *Journal of Chemical Education*, *60*(8), 625.

Keresztury, G., Chalmers, J. M., & Griffith, P. R. (2002). Raman Spectroscopy: Theory in Handbook of Vibrational Spectroscopy, vol. 1. *John Wiley &Sons Ltd*.

Keyes, R. W. (1975). Physical limits in digital electronics. *Proceedings of the IEEE*, *63*(5), 740-767.

Khazaei, M., Arai, M., Sasaki, T., Chung, C. Y., Venkataramanan, N. S., Estili, M., ... & Kawazoe, Y. (2013). Novel electronic and magnetic properties of two-dimensional transition metal carbides and nitrides. *Advanced Functional Materials*, *23*(17), 2185-2192.

Kim, K. S., Zhao, Y., Jang, H., Lee, S. Y., Kim, J. M., Kim, K. S., ... & Hong, B. H. (2009). Large-scale pattern growth of graphene films for stretchable transparent electrodes. *nature*, *457*(7230), 706-710.

Lang, B. (1975). A LEED study of the deposition of carbon on platinum crystal surfaces. *Surface Science*, *53*(1), 317-329

REFERENCES (Continued)

Liang, X., Chang, A. S., Zhang, Y., Harteneck, B. D., Choo, H., Olynick, D. L., & Cabrini, S. (2009). Electrostatic force assisted exfoliation of prepatterned few-layer graphenes into device sites. *Nano letters*, *9*(1), 467-472.

Liang, X., Fu, Z., & Chou, S. Y. (2007). Graphene transistors fabricated via transfer-printing in device active-areas on large wafer. *Nano letters*, *7*(12), 3840-3844.

Liu, H., Liu, Y., & Zhu, D. (2011). Chemical doping of graphene. *Journal of materials chemistry*, *21*(10), 3335-3345.

Lu, X., Huang, H., Nemchuk, N., & Ruoff, R. S. (1999). Patterning of highly oriented pyrolytic graphite by oxygen plasma etching. *Applied Physics Letters*, *75*(2), 193-195.

Marinho, B., Ghislandi, M., Tkalya, E., Koning, C. E., & de With, G. (2012). Electrical conductivity of compacts of graphene, multi-wall carbon nanotubes, carbon black, and graphite powder. *Powder Technology*, *221*, 351-358.

Markov, I. L. (2014). Limits on fundamental limits to computation. *Nature*, *512*(7513), 147-154.

Mattevi, C., Kim, H., & Chhowalla, M. (2011). A review of chemical vapour deposition of graphene on copper. *Journal of Materials Chemistry*, *21*(10), 3324-3334.

Miró, P., Audiffred, M., & Heine, T. (2014). An atlas of two-dimensional materials. *Chemical Society Reviews*, *43*(18), 6537-6554.

MTI Corporation, 2021, CVD Furnaces, https://www.mtixtl.com/TwoZoneRotaryTubeFurnace4inQuartz1200C-OTF-1200X-4-R-II.aspx , Access Date: 30.03.2021

Narula, U., Tan, C. M., & Lai, C. S. (2017). Growth mechanism for low temperature PVD graphene synthesis on copper using amorphous carbon. *Scientific reports*, *7*(1), 1-13.

Nemanich, R. J., Lucovsky, G., & Solin, S. A. (1977). Infrared active optical vibrations of graphite. *Solid State Communications*, *23*(2), 117-120.

Neto, A. C., Guinea, F., Peres, N. M., Novoselov, K. S., & Geim, A. K. (2009). The electronic properties of graphene. *Reviews of modern physics*, *81*(1), 109.

Novoselov, K. S., Geim, A. K., Morozov, S. V., Jiang, D., Katsnelson, M. I., Grigorieva, I., ... & Firsov, A. A. (2005). Two-dimensional gas of massless Dirac fermions in graphene. *Nature*, *438*(7065), 197-200.

Novoselov, K. S., Geim, A. K., Morozov, S. V., Jiang, D., Zhang, Y., Dubonos, S. V., ... & Firsov, A. A. (2004). Electric field effect in atomically thin carbon films. *science*, *306*(5696), 666-669.

Novoselov, K. S., Jiang, D., Schedin, F., Booth, T. J., Khotkevich, V. V., Morozov, S. V., & Geim, A. K. (2005). Two-dimensional atomic crystals. *Proceedings of the National Academy of Sciences*, *102*(30), 10451-10453.

REFERENCES (Continued)

Obraztsov, A. N., Zolotukhin, A. A., Ustinov, A. O., Volkov, A. P., Svirko, Y., & Jefimovs, K. (2003). DC discharge plasma studies for nanostructured carbon CVD. *Diamond and Related Materials*, *12*(3-7), 917-920.

Orofeo, C. M., Ago, H., Hu, B., & Tsuji, M. (2011). Synthesis of large area, homogeneous, single layer graphene films by annealing amorphous carbon on Co and Ni. *Nano Research*, *4*(6), 531-540.

Pan, G., Li, B., Heath, M., Horsell, D., Wears, M. L., Al Taan, L., & Awan, S. (2013). Transfer-free growth of graphene on SiO2 insulator substrate from sputtered carbon and nickel films. *Carbon*, *65*, 349-358.

Panchakarla, L. S., Govindaraj, A., & Rao, C. N. R. (2010). Boron-and nitrogen-doped carbon nanotubes and graphene. *Inorganica Chimica Acta*, *363*(15), 4163-4174.

Papageorgiou, D. G., Kinloch, I. A., & Young, R. J. (2017). Mechanical properties of graphene and graphene-based nanocomposites. *Progress in Materials Science*, *90*, 75-127.

Pat, S., Korkmaz, Ş., & Balbağ, M. Z. (2014). A new deposition technique using reactive thermionic vacuum arc for ZnO thin film production. *Journal of Nanoelectronics and Optoelectronics*, *9*(3), 437-441.

Pauli, W. (1925). Über den Zusammenhang des Abschlusses der Elektronengruppen im Atom mit der Komplexstruktur der Spektren. *Zeitschrift für Physik*, *31*(1), 765-783.

Pauling, L. (1931). The nature of the chemical bond. Application of results obtained from the quantum mechanics and from a theory of paramagnetic susceptibility to the structure of molecules. *Journal of the American Chemical Society*, *53*(4), 1367-1400.

Perdereau, J., & Rhead, G. E. (1971). LEED studies of adsorption on vicinal copper surfaces. *Surface Science*, *24*(2), 555-571.

Pham, V. H., Cuong, T. V., Nguyen-Phan, T. D., Pham, H. D., Kim, E. J., Hur, S. H., ... & Chung, J. S. (2010). One-step synthesis of superior dispersion of chemically converted graphene in organic solvents. *Chemical Communications*, *46*(24), 4375-4377.

Raman, C. V., & Krishnan, K. S. (1928). A new type of secondary radiation. *Nature*, *121*(3048), 501-502.

Rao, R., Podila, R., Tsuchikawa, R., Katoch, J., Tishler, D., Rao, A. M., & Ishigami, M. (2011). Effects of layer stacking on the combination Raman modes in graphene. *Acs Nano*, *5*(3), 1594-1599.

Redkov, A. V., Melehin, V. G., Raskhodchikov, D. V., Reshetov, I. V., Tagantsev, D. K., Zhurikhina, V. V., & Lipovskii, A. A. (2019). Modifications of poled silicate glasses under heat treatment. *Journal of Non-Crystalline Solids*, *503*, 279-283.

Reich, S., & Thomsen, C. (2004). Raman spectroscopy of graphite. *Philosophical Transactions of the Royal Society of London. Series A: Mathematical, Physical and Engineering Sciences*, *362*(1824), 2271-2288.

REFERENCES (Continued)

Reich, S., Maultzsch, J., Thomsen, C., & Ordejon, P. (2002). Tight-binding description of graphene. *Physical Review B*, *66*(3), 035412.

Reina, A., Jia, X., Ho, J., Nezich, D., Son, H., Bulovic, V., ... & Kong, J. (2009). Large area, few-layer graphene films on arbitrary substrates by chemical vapor deposition. *Nano letters*, *9*(1), 30-35.

Shang, N. G., Papakonstantinou, P., McMullan, M., Chu, M., Stamboulis, A., Potenza, A., ... & Marchetto, H. (2008). Catalyst-free efficient growth, orientation and biosensing properties of multilayer graphene nanoflake films with sharp edge planes. *Advanced functional materials*, *18*(21), 3506-3514.

Shin, H. J., Kim, K. K., Benayad, A., Yoon, S. M., Park, H. K., Jung, I. S., ... & Lee, Y. H. (2009). Efficient reduction of graphite oxide by sodium borohydride and its effect on electrical conductance. *Advanced Functional Materials*, *19*(12), 1987-1992.

Skoczylas, P., Gulbinowicz, Z., & Goroch, O. (2020). Microstructure and Properties of Tungsten Heavy Alloy Connections Formed during Sintering with the Participation of the Liquid Phase. *Materials*, *13*(21), 4965.

Somani, P. R., Somani, S. P., & Umeno, M. (2006). Planer nano-graphenes from camphor by CVD. *Chemical Physics Letters*, *430*(1-3), 56-59.

Song, J., Wang, X., & Chang, C. T. (2014). Preparation and characterization of graphene oxide. *Journal of Nanomaterials*, *2014*.

Speyer, L., Fontana, S., Cahen, S., & Hérold, C. (2018). Simple production of high-quality graphene foams by pyrolysis of sodium ethoxide. *Materials Chemistry and Physics*, *219*, 57-66.

Staudenmaier, L. (1898). Verfahren zur darstellung der graphitsäure. *Berichte der deutschen chemischen Gesellschaft*, *31*(2), 1481-1487.

Subrahmanyam, K. S., Panchakarla, L. S., Govindaraj, A., & Rao, C. N. R. (2009). Simple method of preparing graphene flakes by an arc-discharge method. *The Journal of Physical Chemistry C*, *113*(11), 4257-4259.

Subrahmanyam, K. S., Vivekchand, S. R. C., Govindaraj, A., & Rao, C. N. R. (2008). A study of graphenes prepared by different methods: characterization, properties and solubilization. *Journal of Materials Chemistry*, *18*(13), 1517-1523.

Sutter, P. W., Flege, J. I., & Sutter, E. A. (2008). Epitaxial graphene on ruthenium. *Nature materials*, *7*(5), 406-411.

Sutter, P. W., Flege, J. I., & Sutter, E. A. (2008). Epitaxial graphene on ruthenium. *Nature materials*, *7*(5), 406-411.

Tan, P. H., Han, W. P., Zhao, W. J., Wu, Z. H., Chang, K., Wang, H., ... & Ferrari, A. C. (2012). The shear mode of multilayer graphene. *Nature materials*, *11*(4), 294-300.

Venkatarayudu, T. (1954). The rule of mutual exclusion. *The Journal of Chemical Physics*, *22*(7), 1269-1269.

REFERENCES (Continued)

Villa, A., & Dimitratos, N. (Eds.). (2018). *Metal-free functionalized carbons in catalysis: synthesis, characterization and applications* (Vol. 31). Royal Society of Chemistry.

Wallace, P. R. (1947). The band theory of graphite. *Physical review*, *71*(9), 622.

Wang, G., Yang, J., Park, J., Gou, X., Wang, B., Liu, H., & Yao, J. (2008). Facile synthesis and characterization of graphene nanosheets. *The Journal of Physical Chemistry C*, *112*(22), 8192-8195.

Wang, J., Zhu, M., Outlaw, R. A., Zhao, X., Manos, D. M., & Holloway, B. C. (2004). Synthesis of carbon nanosheets by inductively coupled radio-frequency plasma enhanced chemical vapor deposition. *Carbon*, *42*(14), 2867-2872.

Wang, Q. H., Kalantar-Zadeh, K., Kis, A., Coleman, J. N., & Strano, M. S. (2012). Electronics and optoelectronics of two-dimensional transition metal dichalcogenides. *Nature nanotechnology*, *7*(11), 699-712.

Wu, Y. H., Yu, T., & Shen, Z. X. (2010). Two-dimensional carbon nanostructures: Fundamental properties, synthesis, characterization, and potential applications. *Journal of Applied Physics*, *108*(7), 10.

Wu, Z. S., Ren, W., Gao, L., Zhao, J., Chen, Z., Liu, B., ... & Cheng, H. M. (2009). Synthesis of graphene sheets with high electrical conductivity and good thermal stability by hydrogen arc discharge exfoliation. ACS nano, 3(2), 411-417.

Xia, Z. Y., Pezzini, S., Treossi, E., Giambastiani, G., Corticelli, F., Morandi, V., ... & Palermo, V. (2013). The exfoliation of graphene in liquids by electrochemical, chemical, and sonication-assisted techniques: A nanoscale study. *Advanced Functional Materials*, *23*(37), 4684-4693.

Xu, M., Liang, T., Shi, M., & Chen, H. (2013). Graphene-like two-dimensional materials. *Chemical reviews*, *113*(5), 3766-3798.

Yi, M., & Shen, Z. (2015). A review on mechanical exfoliation for the scalable production of graphene. *Journal of Materials Chemistry A*, *3*(22), 11700-11715.

Zhang, J., Yang, H., Shen, G., Cheng, P., Zhang, J., & Guo, S. (2010). Reduction of graphene oxide via L-ascorbic acid. *Chemical communications*, *46*(7), 1112-1114.

Zhang, X., Wang, L., Xin, J., Yakobson, B. I., & Ding, F. (2014). Role of hydrogen in graphene chemical vapor deposition growth on a copper surface. *Journal of the American Chemical Society*, *136*(8), 3040-3047.

Zhang, Y., Small, J. P., Pontius, W. V., & Kim, P. (2005). Fabrication and electric-field-dependent transport measurements of mesoscopic graphite devices. *Applied Physics Letters*, *86*(7), 073104.

Zheng, M., Takei, K., Hsia, B., Fang, H., Zhang, X., Ferralis, N., ... & Javey, A. (2010). Metal-catalyzed crystallization of amorphous carbon to graphene. *Applied Physics Letters*, *96*(6), 063110.

REFERENCES (Continued)

Zhou, X., Zhang, J., Wu, H., Yang, H., Zhang, J., & Guo, S. (2011). Reducing graphene oxide via hydroxylamine: a simple and efficient route to graphene. *The Journal of Physical Chemistry C*, *115*(24), 11957-11961.

Zhu, C., Guo, S., Fang, Y., & Dong, S. (2010). Reducing sugar: new functional molecules for the green synthesis of graphene nanosheets. *ACS nano*, *4*(4), 2429-2437.